PALEOCEANOGRAPHY, VOL. 15, NO. 2, PAGES 210-228, APRIL 2000

Climatically sensitive eolian and hemipelagic deposition in the Cariaco Basin, Venezuela, over the past 578,000 years: Results from Al/Ti and K/Al

K. M. Yarincik and R. W. Murray

Department of Earth Sciences, Boston University, Boston, Massachusetts

L.C. Peterson

Rosenstiel School of Marine and Atmospheric Science, University of Miami, Miami, Florida

Abstract. Al/Ti and K/Al ratios in bulk sediment are used to interpret wind-blown and hemipelagic sources of deposition to a 578 kyr record in the Cariaco Basin, Venezuela (Ocean Drilling Program site 1002). Graphical and cross-spectral analyses indicate that these ratios vary extremely closely with planktonic foraminiferal $\delta^{18}O$, with both ratios being significantly higher during interglacials and lower during glacials. K/Al indicates that during glacials the lower sea level that results in relative basin isolation increases the relative proportion of kaolinite derived from local rivers draining the relatively humid Venezuelan margin. Al/Ti decreases during glacials, suggesting greater proportions of eolian rutile sourced from the northern Sahara (due to increased wind strength and/or aridity). This interpretation is consistent with previous studies of the chemistry and mineralogy of Saharan-derived eolian matter in the Caribbean and with a mass balance determining the effect of changes in eolian rutile accumulation on the bulk sedimentary Al/Ti ratio.

1. Introduction

Terrigenous material is deposited into the ocean via fluvial and eolian pathways [*Rea*, 1994, and references therein]. Both pathways are sensitive to climate; effects of sea level on the exposure of continental shelves can alter the amount and/or path of sediment being transported in the ocean, and the collected variations in aridity, wind strength, and direction can alter the magnitude and nature of eolian fluxes. For example, *Thompson et al.* [1995] and *O'Brien et al.* [1995] linked variations in eolian dust within a tropical and Greenland ice core, respectively, to variations in continental aridity between glacial and interglacial periods, finding a greater amount of terrigenous material during arid glacial periods. Similarly, paleoceanographers elucidate changes in climatic conditions on the basis of studies of terrigenous inputs to marine sediments [e.g., *Sarnthein et al.*, 1981; *Leinen et al.*, 1986; *Leinen*, 1989; *Ruddiman and Janecek*, 1989; *Hovan et al.*, 1991; *Hovan and Rea*, 1992; *deMenocal et al.*, 1993; *Rea*, 1994; *Rea et al.*, 1994, 1998; *Tiedemann et al.*, 1994; *Balsam et al.*, 1995; *Rea and Hovan*, 1995; and references therein].

In concert with paleoceanographic studies of climate sensitivity recorded by higher latitude sediments [e.g., *Oppo et al.*, 1998; *Raymo et al.*, 1998], it is important to compare the sensitivity of other regions to expand our understanding of global variability of the ocean-atmosphere system. The tropics have been shown to be sensitive to glacial conditions [e.g., *Thompson et al.*, 1995], and northern Africa and northern South America [e.g., *Damuth and Fairbridge*, 1970; *Bonatti and Gartner*, 1973; *Sarnthein*, 1978; *Balsam et al.*, 1995] have both been documented to be susceptible to increased wind strength and aridity during glacials. We here examine the record of terrigenous deposition in the Cariaco Basin, a marine basin well-situated to document both eolian and hemipelagic deposition at low latitudes. Through terrigenous source studies in this region, the importance of the role of the tropics in the global climate system may become more clear.

Since Cariaco is situated in the northern equatorial region, it is particularly sensitive to seasonal latitudinal shifting of the Intertropical Convergence Zone (ITCZ), which influences the strength and position of the trade winds [*Hastenrath and Lamb*, 1977]. When the ITCZ is at its southernmost position in Northern Hemisphere winter, the Cariaco Basin is subjected to intensified northeasterly trade winds [*Hastenrath and Lamb*, 1977], which induce Ekman upwelling. During Northern Hemisphere summer, the Cariaco Basin is situated within the ITCZ and is subjected to rains, which act to decrease salinity and increase fluvial discharge, and weak winds associated with the ITCZ. The trade winds carry eolian material from North Africa into the tropical North Atlantic and Caribbean regions

Paper number 1999PA900048.
0883-8305/00/1999PA900048$12.00

[*Glaccum*, 1978; *Prospero et al.*, 1981; *Duce et al.*, 1991; *Tiedemann et al.*, 1994; *Balsam et al.*, 1995]; thus, contribution of eolian material from this source would also be affected by the shifting of the ITCZ.

We document here variations in Al/Ti and K/Al measured on bulk sediment that correspond closely to changes in $\delta^{18}O$ of the planktonic foraminifer *Globigerinoides ruber* and thus to climate. We show that during glacial periods terrigenous matter in the Cariaco Basin is dominated by input from local Venezuelan Rivers and the northern Sahara desert. Therefore, glacial periods are characterized by the relative restriction of the basin and increased Saharan-derived eolian inputs. During interglacials, Saharan-sourced inputs decrease, and higher sea levels result in the decrease of local inputs due to the deepening of channels through which sediment from other regions can enter the basin. This initial investigation, based on sampling at relatively low resolution, explores the connection between climate and sediment chemistry in order to provide a baseline for future higher-resolution studies.

2. Cariaco Basin

The Cariaco Basin (10°40'N, 65°00'W) (Figure 1) is an east-west trending pull-apart basin [*Schubert*, 1982] which consists of two 1400 m deep subbasins separated by a 900 m deep saddle. Ocean Drilling Program (ODP) leg 165 drilled site 1002 on the western side of this saddle. In addition to the significance of its geographic position, the Cariaco Basin has an extremely high sedimentation rate (~30 cm kyr^{-1}) [*Peterson et al.*, 2000], allowing for high- and ultra-high resolution paleoceanographic investigations.

Currently, the Caraico Basin is anoxic below ~300 m water depth, the onset of which occurred ~12.6 ^{14}C kyr ago [*Peterson et al.*, 1991]. This anoxia also contributes to the high sedimentary preservation in that the anoxic sediments are unbioturbated and exist as distinct laminated segments [*Peterson et al.*, 1991, 2000; *Hughen et al.*, 1996]. Anoxic conditions stem from the Cariaco Basin being separated to its north and west from the open Caribbean Sea by the Tortuga Bank and to its east by the shallow platform surrounding the islands of Margarita and Cubagua as well as the Araya peninsula (Figure 1). These shallow sills, each <100 m deep, inhibit basinal circulation and become more significant during maximum sea level lowstands (e.g., glacials), leaving only two narrow channels sufficiently deep to remain submerged. One is on the western edge of the basin (146 m), and the other is on the northern edge (120 m) between Tortuga and Margarita Island [*Peterson et al.*, 1991, and references therein]. Upwelling-induced high production is enhanced during interglacials as rising sea level increases the delivery of nutrients from thermocline depths in the open Caribbean [*Peterson et al.*, 1991; *Haug et al.*, 1998]. Greater relative restriction during glacial times also affects the pathways of sediment entering the basin. Because these varying parameters (e.g., sea level, biologic productivity) are well documented, the basin's sedimentary sequence is yielding critical new insights into tropical climate change.

3. Elemental Ratios

This paper focuses on the distributions of Al, Ti, and K in bulk sediment. The ratio Al/Ti is representative of the crustal fraction since both Al and Ti are refractory elements relatively concentrated in continental rocks [*Taylor and McLennan*, 1985]. Aluminum is a primary constituent of aluminosilicate minerals and the crustal component. Titanium is relatively concentrated in heavy minerals [e.g., *Schutz and Rahn*, 1982], which many have hypothesized is commonly predominantly associated with the coarser sediment fraction [*Boyle*, 1983; *Shimmield et al.*, 1990; *Shimmield and Mowbray*, 1991; *Weedon and Shimmield*, 1991]. Ti is used in a variety of geochemical [e.g., *Brimhall et al.*, 1988] and eolian source

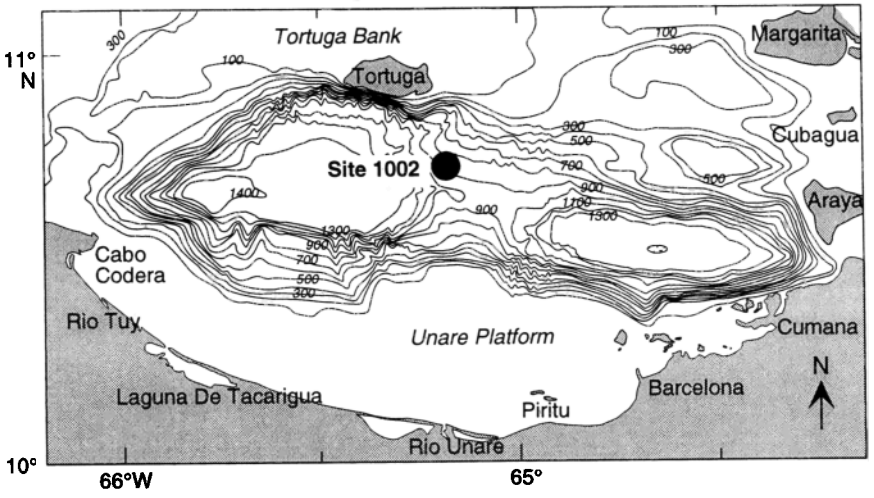

Figure 1. Location of Ocean Drilling Program site 1002 [from *Sigurdsson et al.*, 1997]. Note relatively shallow sill depths encircling the basin.

identification studies (cited above). Aluminum and Ti do not respond to redox variations; thus, Al/Ti variations in Cariaco Basin sediment are not diagenetically controlled. As discussed below, Al in these sediments is not responding to changes in biogenic flux [*Murray et al.*, 1993; *Murray and Leinen*, 1996; *Dymond et al.*, 1997; *Banakar et al.*, 1998] since the "excess" Al component is too low.

In the Cariaco Basin, Al/Ti is potentially representative of grain size, source geochemistry, or both, as has been described for other regions (as cited above). Al/Ti ratios of sources for the terrigenous material in the Cariaco Basin, including local Venezuelan Rivers that drain directly into the basin, the more distant Amazon and Orinoco Rivers, and the deserts of North Africa, range between 11 and 27 (g/g) (Table 1). Illite ($KAl_2(OH)_2[AlSi_3(O,OH)_{10}]$) is generally a weathering product in temperate to arid climates where physical weathering is dominant, while kaolinite ($Al_2O_3 \cdot 2SiO_2 \cdot 2H_2O$) is generally a product of chemical weathering in tropical, humid climates [e.g., *Bonatti and Gartner*, 1973]. Accordingly, we here use K/Al as a proxy for the illite/kaolinite ratio and therefore for the nature of the source of weathered matter being deposited in the basin. We are assisted in this endeavor by comparing our chemical data to the clay mineralogic data of *Clayton et al.* [1999], who performed detailed clay studies on these same ODP cores. As noted by *Boyle* [1983], however, the higher analytical precision of K/Al chemical analyses compared to the clay mineralogy techniques is an advantage.

4. Methods

4.1. Inductively Coupled Plasma Emission Spectrometry

Core samples (approximately two per core section) were freeze-dried and powdered manually in an agate mortar and pestle. Approximately 0.12 g of each sample was digested by microwave digestion and a series of dissolution and evaporation steps involving HNO_3, HF, $HClO_4$, HCl, and H_2O_2, following a procedure similar to that of *Murray and Leinen* [1996]. Once the samples were completely dissolved, solutions were diluted 1000-fold for major element analyses prior to introduction into a Jobin Yvon JY 138 Ultrace inductively coupled plasma emission spectrometer (ICP-ES) in the Analytical Geochemistry Laboratory at Boston University to determine concentrations of Al (measured at λ = 308.215 nm), Ti (λ = 308.802 nm), and K (λ = 766.490 nm). Data were acquired in sequential mode, using background corrections as appropriate, and are not salt-corrected.

Two hundred thirty-five samples were analyzed in nine preparation batches over a period of several months. A homogenized natural sample of average Cariaco Basin sediment was analyzed with each batch as an internal reference and to determine analytical precision. Samples were prepared and analyzed in different random depth orders. A precision of 2% of the measured value was obtained for Al/Ti (20.7 ± 0.4) and 4% for K/Al (0.24 ± 0.01). A standard reference sediment (BCSS-1, an estuarine sediment from Baie des Chaleurs in the Gulf of St. Lawrence) was also analyzed with each batch to confirm analytical accuracy. Accuracy of the reference sediment analysis was within precision of the measurement.

4.2. Age Model and Spectral Analyses

The oxygen isotope ($\delta^{18}O$) data for site 1002, based on the planktonic foraminifer *G. ruber*, and the resultant age model are from *Peterson et al.* [2000]. Biostratigraphic parameters, the construction of a corrected depth scale to account for core expansion, and other information relevant to the construction of the model are also provided by *Peterson et al.* [2000]. The age model is insufficiently resolved to determine elemental mass accumulation rates [*Haug et al.*, 1998] and therefore temporal changes in these rates are not discussed here. Hole 1002C was drilled to a depth of ~170 meters below seafloor (mbsf) and covers an age range of 0 to ~578 kyr. The average age resolution between samples in this study is ~2.5 ± 2 kyr.

Table 1. Al/Ti Data from Potential Terrigenous Sources

Source	Reference	Al/Ti, g/g
Granite	*Condie* [1993]	47
Scavenged biogenic	*Murray and Leinen* [1996]	41
Average upper crust	*Taylor and McLennan* [1985]	27
Inferred fluvial input into Cariaco Basin	This work, based on *Longa and Bonilla* [1987]	27
Post-Archean Average Shale (PAAS)	*Taylor and McLennan* [1985]	17
Amazon River	*Martin and Meybeck* [1979]	16
Amazon River	*Taylor and McLennan* [1985]	16
North Atlantic aerosol, Saharan dust	*Glaccum* [1978]	14
Orinoco River	*Eisma et al.* [1978]	13
Orinoco River	*Martin and Meybeck* [1979]	13
Northern Saharan dust	*Ganor et al.* [1991]	11
Oceanic crust	*Taylor and McLennan* [1985]	9
Average Guiana Shield	*Johnsson et al.* [1991]	6
Ocean island basalts (Marquesas Islands)	*Liotard et al.* [1986]	4

Table 2. Results of Cross-Spectral Analysis, ODP Site 1002, Cariaco Basin

	Phase Difference ± Phase Error; Coherency; kyr Lead or Lag			
Variable 1 Versus Variable 2	100 kyr	41 kyr	23 kyr	19 kyr
$\delta^{18}O$ Versus SPECMAP	2 ± 9; 0.94	-8 ± 8; 0.95	6 ± 10; 0.94	1 ± 7; 0.96
% $CaCO_3$ Versus $\delta^{18}O$	- 157 ± 13; 0.89; 44	163 ± 28; 0.64; 19	----------	----------
Al/Ti Versus $\delta^{18}O$	- 181 ± 7; 0.97; 50	129 ± 26; 0.69; 15	131 ± 14; 0.89; 8	- 214 ± 24; 0.71; 8
K/Al Versus $\delta^{18}O$	- 152 ± 18; 0.80; 42	193 ± 13; 0.89; 19	----------	211 ± 28; 0.65; 8
Al/Ti Versus % $CaCO_3$	- 23 ± 12; 0.90; 6	- 39 ± 13; 0.89; 4	11 ± 24; 0.71; <1	----------
K/Al Versus % $CaCO_3$	13 ± 19; 0.79; 4	22 ± 25; 0.70; 3	----------	7 ± 18; 0.81; <1
Al/Ti Versus K/Al	- 33 ± 22; 0.74; 9	- 60 ± 18; 0.81; 7	----------	----------

Positive phase angles indicate that the first variable leads the second. Coherency equals 0.64 at the 80% confidence level. No phase angle is given if records are not coherent at the 80% confidence level or if one variable shows no increase in variance centered at the period of interest. "Kyr Lead or Lag" was calculated by [(Phase Difference)/360 x Frequency]. Interpolation and cross-spectral analyses were performed for 287 samples at Δt = 2 kyr for 572 kyr. Bandwidth is 0.007 with 95 lags.

Sedimentation rates are extremely high (~30 cm kyr^{-1}) [*Peterson et al.*, 2000]. Because hole 1002C, core 9H, was disturbed, samples from hole 1002D, cores 9H and 10H, were merged with the data from hole 1002C at their respective depths [*Haug et al.*, 1998]. Blackman-Tukey cross-spectral analyses were performed using the ARAND software package available from Brown University. Details of the statistical analyses are provided in the caption of Table 2. Cross-spectral comparison of the $\delta^{18}O$ record from site 1002 to the SPECMAP isotopic stack [*Imbrie et al.*, 1984] indicates high coherence and no phase offsets at the 100 kyr, 41 kyr, 23 kyr, and 19 kyr Milankovitch periods (Table 2).

5. Results

All chemical data are provided in Table 3.[1]

5.1. Terrigenous Matter

The concentration of terrigenous matter (Figure 2; Table 3) was determined using both a Ti-based and Al-based normative calculation [*Murray and Leinen*, 1996, and references therein]. For Ti, the calculation is

$$\% \text{ terrigenous} = (Ti_{sample} / Ti_{PAAS}) \times 100.$$

This calculation assumes that the terrigenous component of sediment is compositionally similar to Post Archean Average Shale (PAAS) with respect to Ti. Ti is relatively constant in shales [*Murray and Leinen*, 1996, and references therein]; however, considering the variations in the eolian input of Ti that are discussed below, this calculation was also performed using Al. There are no significant differences between the Ti-based and Al-based calculations in the temporal pattern of terrigenous concentration (Figure 2). The average of the Ti-based and Al-based calculations (Table 3) indicates that the abundance of terrigenous matter ranges between 36 weight percent (wt %) (minimum at ~301 kyr) and 91 wt % (maximum at ~337 kyr) and averages 64 ± 11 wt. %.

The amount of continentally derived material covaries with $\delta^{18}O$ and is generally higher during glacials. The concentration of terrigenous matter varies negatively with $CaCO_3$ (Figure 2), which most likely reflects a dilution relationship between these components. Cross spectral analysis between $CaCO_3$ (wt %) and $\delta^{18}O$ indicates that periods of low carbonate concentration occur during glacials, an observation that has been previously interpreted as recording the advection of nutrient-poor surface waters into the Cariaco Basin during low sea level stands [*Peterson et al.*, 2000, and references therein].

5.2. Al/Ti, K/Al, and Cross-Spectral Analyses

Al/Ti varies downcore (Figure 3; Table 3), ranging from 17.5 to 23.5 and averaging 20.2 ± 1.2, with values being significantly higher during interglacial periods and lower during glacials. Al/Ti closely follows $\delta^{18}O$ throughout the entire record. This relationship is extremely strong, with even small scale variations in Al/Ti mimicking the $\delta^{18}O$ variations (Figure 3). This close relationship readily apparent in graphical form is confirmed by cross-spectral analysis (Figure 4; Table 2), which documents coherence between high Al/Ti and low $\delta^{18}O$ at all Milankvitch frequencies. This is especially true in the 100 kyr band, which is the strongest cross-spectral

[1] Table 3 is available electronically at World Data Center-A for Paleoceanography, NOAA/NGDC, 325 Broadway, Boulder, Colorado (email: paleo@mail.ngdc.noaa.gov; URL: http://www.ngdc.noaa.gov/paleo).

Table 3. Results From Chemical Analyses on Bulk Sediment From ODP Site 1002, Cariaco Basin

Sample (Hole-Core-Section-Interval)	Depth, mbsf	Age, kyr	Al, wt %	Ti, ppm	K, wt %	Al/Ti, g/g	K/Al, g/g	Terrigenous, wt %
C-1H-1-47-49	0.47	1.253	5.52	2472	1.37	22.3	0 25	48
C-1H-1-105-107	1.05	2.671	5.59	2503	1.26	22.3	0.23	49
C-1H-2-46-48	1.96	4.705	5.73	2609	1.25	22.0	0.22	50
C-1H-2-105-107	2.55	6.025	6.34	2837	1.39	22.3	0.22	55
C-1H-3-46-48	3.46	8.059	6.43	2991	1.57	21.5	0.24	57
C-1H-3-105-107	4.05	9.379	5.04	2525	1.31	19.9	0.26	46
C-1H-4-46-48	4.96	11.413	4.57	2326	1.20	19.7	0.26	42
C-1H-4-126-128	5 76	13.202	5.24	2474	1.31	21.2	0.25	47
C-1H-5-27-29	6.27	14.342	6.98	3220	1.40	21.7	0.20	62
C-1H-5-66-68	6.66	14.974	7.54	3607	1.60	20.9	0.21	68
C-1H-5-106-108	7.06	15.449	9.57	5103	1.78	18.8	0.19	90
C-1H-6-7-9	7.57	16.056	10.13	5798	1.80	17.5	0.18	99
C-1H-6-63-65	8.13	16.722	7.32	3636	1.44	20.1	0.20	67
C-2H-1-47-49	8.87	17.243	7.51	3828	1.40	19.6	0.19	69
C-2H-1-123-125	9.63	17.681	7.35	4044	1.39	18.2	0.19	70
C-2H-2-47-49	10.37	18.107	7.52	4004	1.43	18.8	0.19	71
C-2H-2-123-125	11.13	18.551	7.51	3954	1.52	19.0	0 20	71
C-2H-3-47-49	11.87	18.976	8.29	4286	1.54	19.4	0.19	77
C-2H-3-123-125	12.63	19.414	7.96	4228	1.54	18.8	0.19	75
C-2H-4-47-49	13.37	19.840	7.73	3940	1.57	19.6	0.20	72
C-2H-4-123-125	14.13	20.917	6.33	3115	1.29	20.3	0.20	58
C-2H-5-47-49	14.87	22.341	7.68	4064	1.53	18.9	0.20	72
C-2H-5-123-125	15.63	23.785	6.06	3141	1.29	19.3	0 21	57
C-2H-6-47-49	16.37	25.189	7.79	4047	1.46	19.2	0 19	73
C-2H-6-123-125	17.13	26.633	7.00	3614	1 12	19.4	0.16	65
C-2H-7-7-9	17.47	27.296	8.01	4208	1 55	19.0	0.19	75
C-3H-1-14-16	18.04	28.369	8.80	4551	1 59	19.3	0.18	82
C-3H-1-110-112	19.00	30.524	6.21	2989	1.25	20.8	0.20	56
C-3H-2-10-12	19.50	31.426	7.00	3608	1.43	19.4	0.20	65
C-3H-2-112-114	20.52	33.239	6.94	3843	1.44	18.1	0.21	67
C-3H-3-15-17	21.05	34.206	7.79	3816	1.60	20.4	0.21	71
C-3H-3-111-113	22.01	35.915	8.59	4492	1.63	19.1	0.19	80
C-3H-4-25-27	22.68	37.117	7.22	3742	1.56	19.3	0.22	67
C-3H-4-112-114	23.55	39.195	7.39	3918	1.50	18.9	0.20	70
C-3H-5-92-94	24.85	43.216	7.35	3723	1.48	19.7	0.20	68
C-3H-6-45-47	25.91	46.478	8.00	4097	1.54	19.5	0.19	74
C-3H-6-94-96	26.40	47.996	8.75	4665	1.67	18.7	0.19	83
C-4H-1-67-69	28.07	54.520	7.09	3500	1.52	20.2	0.21	65
C-4H-1-123-125	28.63	56.232	9.15	4789	1.72	19.1	0.19	86
C-4H-2-67-69	29.57	59.107	7.87	3905	1.62	20.2	0.21	72
C-4H-2-123-125	30.13	60.819	8.50	4332	1.62	19.6	0.19	79
C-4H-3-67-69	31.10	63.822	8.59	4273	1.68	20.1	0.20	79
C-4H-3-123-125	31.66	66.988	9.03	4378	1.77	20.6	0.20	82
C-4H-4-67-69	32.67	70.360	8.95	4318	1.81	20.7	0.20	81
C-4H-4-123-125	33.23	72.596	9.29	4592	1.86	20.2	0.20	85
C-4H-5-67-69	34.28	76.875	8.01	3820	1.64	21 0	0.20	72
C-4H-5-123-125	34.84	79.142	7.28	3453	1.51	21 1	0.21	65
C-4H-6-67-69	35.81	83.078	7.91	3788	1.62	20.9	0.20	71
C-4H-6-123-125	36.37	85.346	8.55	4113	1.78	20.8	0 21	77
C-4H-7-46-48	37.10	88.319	7.97	4006	1.59	19.9	0.20	73
C-5H-1-18-20	37.08	90.266	7.65	3695	1.59	20.7	0.21	69
C-5H-1-113-115	38.03	94.031	7.28	3162	1.47	23.0	0 20	63
C-5H-2-18-20	38.58	96.255	7.84	3608	1.60	21.7	0 20	69
C-5H-2-113-15	39.53	100.020	8.06	3883	1.66	20.8	0.21	73
C-5H-3-18-20	40.08	102.223	8.20	3976	1.72	20.6	0.21	74
C-5H-3-113-115	41.03	106.010	8.17	3846	1.73	21.2	0.21	73
C-5H-4-15-17	41.62	108.363	7.04	3195	1.69	22.0	0.24	62

Table 3. (continued)

Sample (Hole-Core-Section-Interval)	Depth, mbsf	Age, kyr	Al, wt %	Ti, ppm	K, wt %	Al/Ti, g/g	K/Al, g/g	Terrigenous, wt %
C-5H-4-113-115	42.60	112.256	6.54	3001	1.41	21.8	0.22	58
C-5H-5-16-18	43.13	114.395	6.85	3155	1.49	21.7	0.22	61
C-5H-5-113-115	44.10	118.246	6.50	2904	1.48	22.4	0.23	57
C-5H-6-15-17	44.62	120.342	7.64	3489	1.60	21.9	0.21	67
C-5H-6-113-115	45.60	124.235	6.35	3122	1.43	20.3	0.23	58
C-5H-7-18-20	46.15	126.417	7.15	3716	1.62	19.2	0.23	67
C-6H-1-15-17	46.55	128 044	6.77	3589	1.45	18 9	0.21	64
C-6H-2-56-58	47.23	133.539	7.34	3616	1 49	20.3	0.20	67
C-6H-2-112-114	47.79	135.736	7.40	3693	1.48	20.0	0.20	68
C-6H-3-56-58	48.73	139.473	10.25	5191	1.97	19.7	0.19	95
C-6H-3-101-103	49.18	141.231	7.38	3633	1.50	20.3	0.20	67
C-6H-4-56-58	50.23	145.385	7.89	3930	1.54	20.1	0.20	72
C-6H-4-112-114	50.79	147.604	7.58	3844	1.49	19.7	0.20	70
C-6H-5-55-57	51.72	151.297	7.81	4031	1.52	19.4	0.19	73
C-6H-5-111-113	52.28	153.048	8.35	4332	1.58	19.3	0.19	78
C-6H-6-55-57	53.27	155.792	7 82	3901	1.58	20.0	0.20	72
C-6H-6-112-114	53.84	157.365	7.74	4235	1.51	18.3	0.20	74
C-6H-7-55-57	54.82	160.078	8.36	4776	1.66	17.5	0.20	82
C-6H-7-111-113	55.38	161.651	8.89	4579	1.74	19.4	0.20	83
C-6H-8-54-56	56.31	164.225	8.58	4788	1.71	17.9	0.20	83
C-7H-1-35-37	56.25	166.923	8.20	4364	1.64	18.8	0.20	77
C-7H-1-63-65	56.53	167.663	9.31	4974	1.87	18.7	0.20	88
C-7H-2-35-37	57.13	169.205	9.20	5114	1.84	18.0	0.20	89
C-7H-2-124-126	58.02	171.486	8.64	4575	1.75	18.9	0.20	81
C-7H-3-35-37	58.63	173.059	8.33	4587	1.72	18.2	0.21	80
C-7H-3-130-132	59.58	175.525	9.26	4710	1.86	19.7	0 20	86
C-7H-4-53-55	60.31	177.406	8.69	4590	1.71	18.9	0.20	82
C-7H-4-134-136	61.12	179.487	9.40	5020	1.90	18.7	0.20	89
C-7H-5-35-37	61.70	180.983	9.55	4940	1.89	19.3	0.20	89
C-7H-5-124-126	62.59	182.539	8.83	4609	1.80	19.2	0.20	83
C-7H-6-24-26	63.14	183.129	7.95	4064	1.65	19.6	0.21	74
C-7H-6-135-137	64.25	184.317	8.84	4513	1.70	19.6	0.19	82
C-7H-7-35-37	64.84	184.958	8.51	4202	1.67	20.3	0.20	78
C-7H-7-115-117	65.64	185.818	9.36	4552	1.89	20.6	0.20	85
C-7H-8-16-18	66.15	186.357	9.84	4729	2.00	20.8	0.20	89
C-7H-8-79-81	66.78	187.037	9.76	4885	2.06	20.0	0.21	90
C-8H-1-18-20	65.58	187.750	9.32	4154	1.87	22.4	0.20	81
C-8H-2-17-19	66.12	188.359	8.13	3779	1.72	21.5	0.21	72
C-8H-2-133-135	67.28	189.643	8.73	4087	1.77	21.4	0.20	78
C-8H-3-17-19	67.62	190.028	9.13	4221	1.85	21.6	0.20	81
C-8H-3-131-133	68.76	191.298	7.36	3622	1.42	20.3	0.19	67
C-8H-4-17-19	69.12	191.696	8.69	4214	1.71	20.6	0.20	79
C-8H-4-132-134	70.27	192.980	6.88	3226	1.45	21.3	0.21	61
C-8H-5-17-19	70.62	193.365	6.68	3087	1.43	21.7	0.21	59
C-8H-5-132-134	71.77	196.264	6.25	2858	1.23	21.9	0.20	55
C-8H-6-17-19	72.15	197.759	6.29	3046	1.36	20.6	0.22	57
C-8H-6-123-125	73.21	201.925	7.32	3922	1.49	18.7	0.20	69
C-8H-7-17-19	73.65	203.645	8 47	4522	1.78	18.7	0.21	80
D-9H-3-25-27	74.13	205.547	7.06	3388	1.45	20.8	0.21	64
C-8H-7-132-134	74.80	209.750	6.91	3475	1.38	19.9	0.20	64
D-9H-3-124-126	75.12	211.938	6.81	3062	1.45	22.2	0.21	60
C-8H-8-17-19	75.15	212.172	7.35	3540	1.47	20.8	0.20	66
D-9H-4-18-20	75.56	214.906	6.69	3061	1.35	21.8	0.20	59
D-9H-4-115-117	76.53	226.512	6.01	2946	1.07	20.4	0.18	55
D-9H-5-12-14	77.00	229.035	6.76	3228	1.40	20.9	0.21	61
D-9H-5-109-111	77.97	235.517	6.12	3038	1.39	20.1	0.23	56
D-9H-6-24-26	78.62	239.117	6.34	3267	1.36	19.4	0.21	59

Table 3. (continued)

Sample (Hole-Core-Section-Interval)	Depth, mbsf	Age, kyr	Al, wt %	Ti, ppm	K, wt %	Al/Ti, g/g	K/Al, g/g	Terrigenous, wt %
D-9H-6-116-118	79.54	242.759	7.72	4052	1.50	19.1	0.19	72
D-9H-7-33-35	80.21	245.448	7.23	3943	1.52	18.3	0.21	69
D-10H-1-19-21	80.89	248.179	6.67	3540	1.29	18.8	0.19	63
D-9H-7-123-125	81.11	249.048	7.48	3976	1.48	18.8	0.20	71
D-9H-8-38-40	81.76	252.207	7.95	4352	1.61	18.3	0.20	76
D-10H-2-57-59	81.84	252.648	6.85	3482	1.47	19.7	0.21	63
D-10H-2-116-118	82.43	255.793	6.12	2983	1.23	20.5	0.20	55
D-10H-3-32-34	83.09	260.087	5.91	2929	1.28	20 2	0.22	54
D-10H-3-117-119	83.94	267.261	7.87	4078	1.56	19 3	0.20	73
C-10H-1-32-34	84.72	273.537	8.65	4464	1.69	19.4	0.20	80
D-10H-4-117-119	85.44	276.607	6.58	3209	1.37	20.5	0.21	60
C-10H-2-24-26	85.45	276.656	7.45	3689	1.48	20.2	0.20	68
C-10H-2-102-104	86.23	279.923	4.57	2184	1.08	20 9	0.24	41
C-10H-3-18-20	86.89	282.723	7.15	3455	1.38	20.7	0.19	65
C-10H-3-99-101	87.70	286.137	6.63	3153	1.28	21.0	0.19	59
C-10H-4-28-30	88.49	289.477	6.39	2939	1.29	21 7	0.20	56
C-10H-4-104-106	89.25	292.719	7.92	3795	1.50	20.9	0.19	71
C-10H-5-23-25	89.99	295.814	6.86	3309	1.40	20.7	0.20	62
C-10H-5-104-106	90.80	299.550	7.38	3636	1.44	20.3	0.19	67
C-10H-6-24-26	91.57	303.674	6.73	3194	1.29	21.1	0.19	60
C-10H-6-133-135	92.66	309.473	7.24	3509	1.46	20.6	0.20	65
C-10H-7-26-28	93.09	311.798	7.65	3599	1.50	21.2	0.20	68
C-10H-7-112-114	93.95	316.388	6.72	2947	1.33	22 8	0.20	58
C-10H-8-32-34	94.65	320.140	6.93	3118	1.32	22.2	0 19	61
C-11H-2-20-22	94.33	326.713	7.89	3391	1.68	23.3	0 21	68
C-11H-2-93-95	95.06	330.219	6.20	2832	1.53	21.9	0.25	55
C-11H-3-45-47	96.08	331.767	6.27	2890	1.34	21.7	0.21	55
C-11H-3-125-127	96.88	332.996	5.54	3009	1.31	18.4	0.24	53
C-11H-4-9-11	97.27	333.585	4.06	2198	0.99	18.5	0.24	39
C-11H-4-56-58	97.74	334.300	4.54	2467	1.15	18.4	0.25	43
C-11H-4-113-115	98.31	335.167	4.09	2150	0.97	19.0	0.24	38
C-11H-5-24-26	99.12	336.396	9.80	5473	1.99	17.9	0.20	95
C-11H-5-99-101	99.87	337.540	8.79	4845	1.71	18.1	0.19	84
C-11H-6-37-39	100.86	339.055	9.98	5451	1.87	18.3	0.19	95
C-11H-6-96-98	101.45	339.947	9.95	5310	1.78	18.7	0.18	94
C-11H-7-70-72	102.72	341.882	8.19	4225	1.55	19.4	0.19	76
C-11H-7-124-126	103.26	343.600	7.40	3854	1.50	19.2	0.20	69
C-11H-8-31-33	103.83	345.543	8.74	4222	1.59	20.7	0.18	79
C-12H-1-18-20	103.58	348.095	7.51	3981	1.41	18.9	0.19	71
C-12H-1-112-114	104.52	351.143	8.04	4114	1.56	19.5	0.19	74
C-12H-2-33-35	105.00	352.705	7.91	3939	1.60	20.1	0.20	72
C-12H-2-109-111	105.76	354.812	8.55	4468	1.70	19.1	0.20	80
C-12H-3-47-49	106.64	356.843	8.82	4462	1.72	19.8	0.19	81
C-12H-3-124-126	107.41	358.604	8.09	4031	1.55	20.1	0.19	74
C-12H-4-42-44	108.09	360.161	9.19	4742	1.68	19.4	0.18	86
C-12H-4-119-121	108.86	361.934	8.21	4179	1.54	19.7	0.19	76
C-12H-5-33-35	109.50	363.397	8.24	4218	1.61	19.5	0.20	76
C-12H-5-127-129	110.44	365.563	8.63	4320	1.64	20.0	0.19	79
C-12H-6-27-29	111.00	366.836	7.89	4145	1.55	19.0	0.20	74
C-12H-6-125-127	111.98	369.581	7.81	3668	1.54	21 3	0.20	70
C-12H-7-55-57	112.78	372.269	8.09	3745	1.57	21.6	0.19	72
C-12H-7-118-120	113.41	374.383	8.18	3937	1.60	20.8	0.20	74
C-12H-8-19-21	113.92	376.103	8.16	3907	1.55	20.9	0.19	73
C-13H-1-50-52	113.40	381.500	8.69	4234	1.76	20.5	0.20	79
C-13H-1-89-91	113.79	383.704	9.02	4270	1.85	21.1	0.21	81
C-13H-2-27-29	114.28	386.491	7.81	3574	1.66	21.8	0.21	69
C-13H-2-121-123	115.22	391.806	7.05	3202	1.43	22.0	0.20	62

Table 3. (continued)

Sample (Hole-Core-Section-Interval)	Depth, mbsf	Age, kyr	Al, wt %	Ti, ppm	K, wt %	Al/Ti, g/g	K/Al, g/g	Terrigenous, wt %
C-13H-3-16-18	115.67	394.333	6.57	2993	1.28	21.9	0.20	58
C-13H-3-121-123	116.72	400.296	6.07	2669	1.22	22.7	0.20	53
C-13H-4-28-30	117.29	403.537	6.29	2818	1.28	22.3	0.20	55
C-13H-4-121-123	118.22	408.158	5.59	2380	1.19	23.5	0.21	48
C-13H-5-36-38	118.87	411.018	6.05	2765	1.37	21.9	0.23	53
C-13H-5-121-123	119.72	414.731	6.48	2936	1.38	22.1	0.21	57
C-13H-6-29-31	120.30	417.416	6.22	2929	1.32	21.2	0 21	56
C-13H-6-124-126	121.25	421.455	7.66	3800	1.52	20.2	0.20	70
C-13H-7-15-17	121.66	423.262	6 72	3036	1.38	22 1	0 21	59
C-13H-7-122-124	122.73	427.928	8.41	4181	1 62	20 1	0.19	77
C-14H-1-23-25	122 63	433.498	8.21	4311	1.60	19.0	0.19	77
C-14H-2-35-37	123 35	437.900	7.91	3918	1 55	20.2	0.20	72
C-14H-2-126-128	124.26	443.825	8.53	4185	1 63	20 4	0.19	78
C-14H-3-35-37	124.85	447.650	8.45	4243	1.61	19.9	0.19	78
C-14H-3-126-128	125.76	453.538	8.22	4157	1.52	19.8	0 19	76
C-14H-4-35-37	126.35	457.325	7.73	3898	1.48	19.8	0.19	71
C-14H-4-126-128	127.26	463.250	8.82	4576	1.54	19.3	0.17	82
C-14H-5-35-37	127.92	467.525	8.84	4529	1.65	19.5	0.19	82
C-14H-5-126-128	128.83	470.672	8.86	4540	1.59	19.5	0.18	82
C-14H-6-35-37	129.51	471.533	8.82	4410	1.63	20.0	0.19	81
C-14H-6-107-109	130.23	472.438	7.94	3947	1.47	20.1	0.19	73
C-15H-1-25-27	132.15	476.744	8.47	4187	1.63	20.2	0.19	77
C-15H-2-25-27	132.82	477.591	7.24	3644	1.37	19.9	0.19	67
C-15H-2-99-101	133.56	478.525	8.66	4218	1.65	20.5	0.19	78
C-15H-3-25-27	134.32	479.489	7.87	3891	1.45	20.2	0.18	72
C-15H-3-99-101	135.06	480.423	8.64	4231	1.65	20.4	0.19	79
C-15H-4-99-101	136.56	482.670	8.23	3926	1.57	21.0	0.19	74
C-15H-5-25-27	137.32	484.678	7.93	3728	1.52	21.3	0.19	71
C-15H-5-99-101	138.06	486.626	6.31	3129	1.31	20.2	0.21	58
C-15H-6-25-27	138.85	488.696	6.75	3252	1.28	20.8	0 19	61
C-15H-6-99-101	139.59	490.675	7.12	3237	1.40	22.0	0.20	63
C-15H-7-25-27	140.20	492.257	7.11	3303	1.14	21.5	0.16	63
C-15H-7-87-89	140.82	493.901	6.75	3195	1.46	21.1	0.22	60
C-16H-1-25-27	141.65	499.958	7.36	3641	1.46	20.2	0.20	67
C-16H-2-18-20	142.15	501.297	6.68	3390	1.29	19.7	0.19	62
C-16H-2-125-127	143.22	504.158	7.14	3679	1.36	19.4	0.19	66
C-16H-3-6-8	143.53	504.980	7.14	3627	1.42	19.7	0.20	66
C-16H-3-125-127	144.72	508.146	7.29	3565	1.36	20.5	0.19	66
C-16H-4-27-29	145.24	509.546	7.56	3802	1.44	19.9	0.19	69
C-16H-4-125-127	146.22	512.164	6.41	3214	1.33	19.9	0.21	59
C-16H-5-25-27	146.72	513.503	6.35	2994	1.17	21.2	0.18	57
C-16H-5-125-127	147.72	516.151	6.75	3427	1.37	19.7	0.20	62
C-16H-6-25-27	148.22	517.490	6.66	3302	1.36	20.2	0.20	61
C-16H-6-125-127	149.22	520.169	7.51	3691	1.49	20.3	0.20	68
C-16H-7-20-22	149.67	521.371	7.45	3614	1.44	20.6	0.19	67
C-16H-7-87-89	150.34	523.151	5.52	2662	1.23	20.8	0.22	50
C-17H-1-31-33	151.21	529.087	8.27	4144	1.53	19.9	0.19	76
C-17H-1-103-105	151.93	531.157	8.07	3988	1.58	20.2	0.20	74
C-17H-2-31-33	152.79	533.622	7.93	3881	1.48	20.4	0.19	72
C-17H-2-129-131	153.77	536.422	8.51	4237	1.62	20.1	0.19	78
C-17H-3-31-33	154.35	538.096	8.85	4378	1.73	20.2	0.20	81
C-17H-3-103-105	155.07	540.166	9.08	4535	1.78	20.0	0.20	83
C-17H-4-31-33	155.93	542.631	8.43	4168	1.67	20.2	0.20	77
C-17H-4-103-105	156.65	544.671	9.66	4670	1.83	20.7	0.19	87
C-17H-5-31-33	157.48	547.075	10.94	5275	2.00	20.7	0.18	99
C-18H-1-28-30	160.68	557.942	9.22	4392	1.71	21.0	0.19	83
C-18H-1-130-132	161.70	560.909	8.44	4268	1.60	19.8	0.19	78

Table 3. (continued)

Sample (Hole-Core-Section-Interval)	Depth, mbsf	Age, kyr	Al, wt %	Ti, ppm	K, wt %	Al/Ti, g/g	K/Al, g/g	Terrigenous, wt %
C-18H-2-28-30	162.18	562.309	8.09	4057	1.57	19.9	0.19	74
C-18H-2-130-132	163.20	565.277	8.96	4408	1.64	20.3	0.18	82
C-18H-3-28-30	163.68	566.677	7.53	3747	1.44	20.1	0.19	69
C-18H-3-130-132	164.70	569.660	8.52	4063	1.57	21.0	0.18	77
C-18H-5-32-34	165.70	572.582	7.08	3532	1.37	20.0	0.19	65
C-18H-5-130-132	166.68	575.413	7.59	3660	naf	20.7	naf	68
C-18H-6-32-34	167.20	576.935	7.86	3730	1.59	21.1	0.20	70

All samples from ODP Leg 165, site 1002. Data overspecified for calculation purposes. 'naf' means 'not analyzed for'.

relationship (coherency = 0.97) observed in the entire data set, even with respect to the $\delta^{18}O$ - SPECMAP comparison (Table 2). Although the visual relationship between Al/Ti and $\%CaCO_3$ (Figure 5) is not as dramatic as between Al/Ti and $\delta^{18}O$ (Figure 3), the cross-spectral analysis suggests strong correlations between these variables in the 100 kyr and 41 kyr band, with Al/Ti only minimally lagging $\%CaCO_3$, and a weaker coherency at 23 kyr (yet with no phase offset).

Values for K/Al range from 0.16 to 0.26, averaging 0.20 ± 0.02 (Figure 6; Table 3). The variations in K/Al also follow $\delta^{18}O$, with the ratio increasing during interglacials and decreasing during glacials, although in general these relationships are not as robust as those between Al/Ti and $\delta^{18}O$. Cross-spectral analysis indicates high K/Al is significantly coherent (and within phase error) with low $\delta^{18}O$ in the 100 and 41 kyr bands, and is only marginally coherent with low $\delta^{18}O$ in the 19 kyr band (Table 2). Unlike the case with Al/Ti and $\%CaCO_3$, K/Al and $\%CaCO_3$ are positively correlated at all periods except for 23 kyr.

Because both Al/Ti and K/Al display strong relationships to the $\delta^{18}O$ and $\%CaCO_3$ records, they also covary with respect to each other. This covariance is perhaps not unexpected, given that the concentration of Al is included in the calculation of both. However, these variations are not caused solely by changes in Al; note that low Al/Ti corresponds with low K/Al. Because Al is in the numerator of one ratio and in the denominator of the other, were Al the dominant influence then these ratios would be inversely, not positively, related. A simple linear comparison of the two ratios indicates essentially no correlation ($r^2 = 0.04$), further indicating that one single variable is not causing their broadly mutual temporal patterns. Cross-spectral analysis indicates that Al/Ti lags behind K/Al at the 100 kyr and 41 kyr frequencies and that these relationships are relatively coherent (Table 2).

6. Eolian and Hemipelagic Deposition in the Cariaco Basin

6.1. Bulk Al/Ti as an Indicator of Terrigenous Matter

Given that the bulk Al/Ti record of some biogenic-rich marine sediment and settling particles includes an Al_{excess} component [*Murray et al.*, 1993; *Murray and Leinen*, 1996; *Dymond et al.*, 1997; *Banaker et al.*, 1998], it is important to define under what conditions this Al_{excess} component is likely to be quantitatively significant. In this study, we are using bulk Al/Ti not as an indicator of upper water column biologic processes, but rather as an indicator of the character of the detrital component.

What is the maximum amount of lithogenic material that can be present in a bulk sediment before the Al_{excess} component is obscured by the detrital load? On the basis of bulk Al/Ti in surface sediment across the equatorial upwelling and productivity maximum in the central equatorial Pacific Ocean [*Murray and Leinen*, 1996], we have calculated that bulk Al/Ti values greater than potential detrital sources can be observed only in sediment with <5% terrigenous matter. To be conservative, we could limit ourselves further to considering only sediment with less than 3-4 wt % terrigenous matter.

As described above, the sediment from the Cariaco Basin contains several tens of weight percent terrigenous matter. Therefore, the variations we observe in bulk Al/Ti at site 1002 are recording only fractionation processes intrinsic to variability within the detrital component and are unrelated to variations in biogenic particle production.

6.2. Local Fluvial Sources

There are no Ti data available regarding the chemistry of local rivers (Tuy, Unare, Neveri, Manzanares, Yaracuy) that drain directly into the Cariaco Basin. Basalts and rocks from the Guiana Shield are relatively Ti-rich (Table 1), and if such sources are local then they could be supplying appropriately Ti-rich sediment to the Cariaco Basin. The Guiana Shield, however, is exposed south of the Orinoco River [*Banks*, 1975], and the small rivers flowing northward into the Cariaco Basin drain a different watershed. Immediately to the south and southeast of the Cariaco Basin is the Serrania del Interior, which consists of undifferentiated folded miogeosynclinal middle Cretaceous to Neogene sediments [*Biju-Duval et al.*, 1982], which are highly unlikely to consist of Ti-rich material [e.g., *Taylor and McLennan*, 1985]. The Villa de Cura district to the west-southwest (and well inland) of the Cariaco Basin includes highly tectonized and low-grade metamorphosed mafic basalts, but these are calc-alkaline in composition and are specifically described as being low in Ti [*Donnelly et al.*,

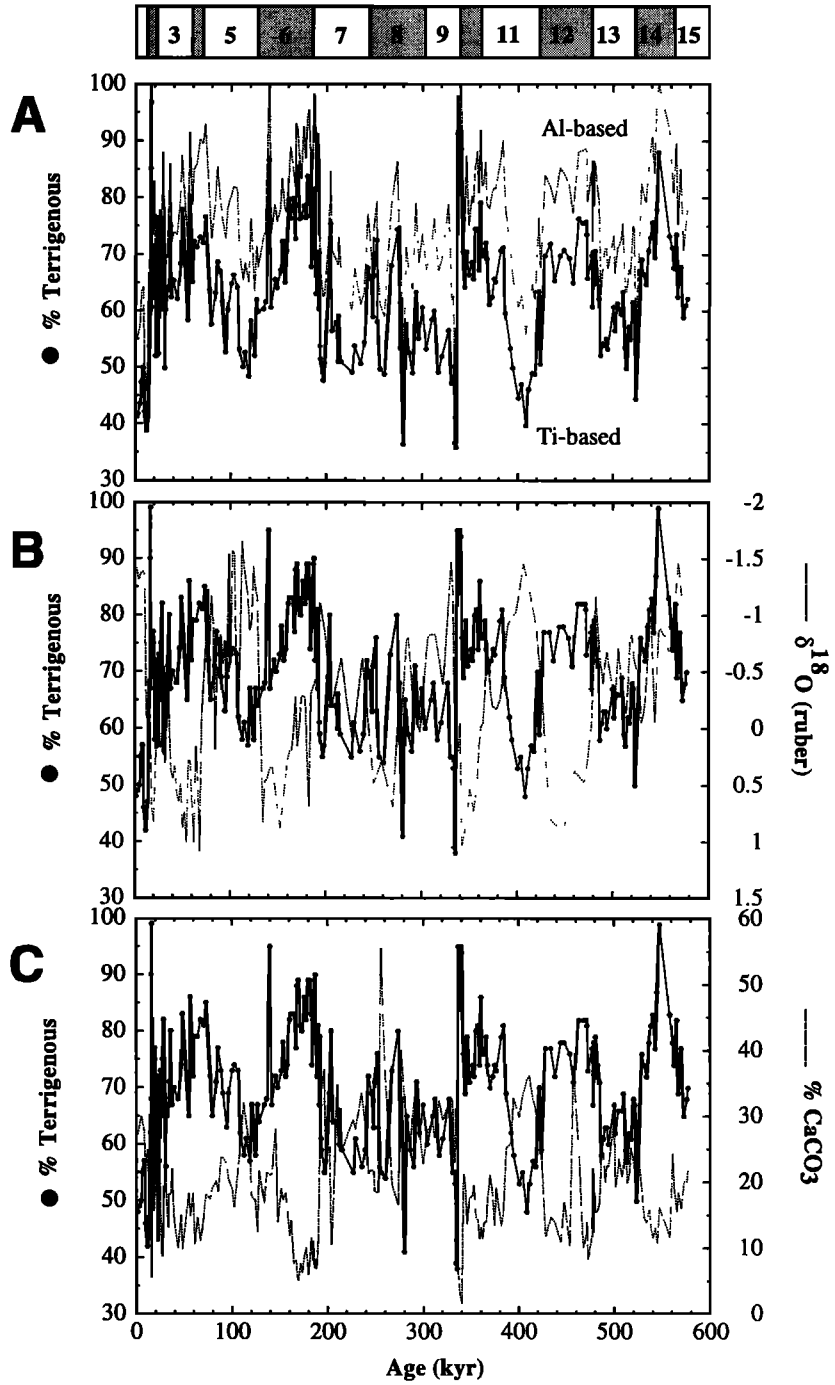

Figure 2. (a) Ti- and Al-based calculations of concentration of terrigenous matter (weight percent). (b) Average concentration of terrigenous matter and $\delta^{18}O$ versus age. (c) Average concentration of terrigenous matter and $CaCO_3$ (weight percent) versus age. Glacial and interglacial (shaded) stages are from *Imbrie et al.* [1984]. $CaCO_3$ (weight percent) from *Peterson et al.* [2000]. $\delta^{18}O$ is plotted at 2 kyr steps as interpolated from the higher-resolution age model of *Peterson et al.* [2000].

1990]. Therefore, we believe there are no geologic formations in the area that could supply material that is suitably enriched in Ti enough to explain the low Al/Ti values in the Cariaco Basin.

Furthermore, while the lack of fluvial Ti data restricts our ability to assign unique sources to the Al/Ti inputs, we are able to at least minimize this limitation by comparing the chemistry that is available for these local sources to representative average crustal sources and therefore at least estimate anticipated Ti concentrations. In particular, on the basis of a survey of available data, we use Fe/Al to infer what Al/Ti may be. Fe/Al ratios for Laguna de Unare sediments

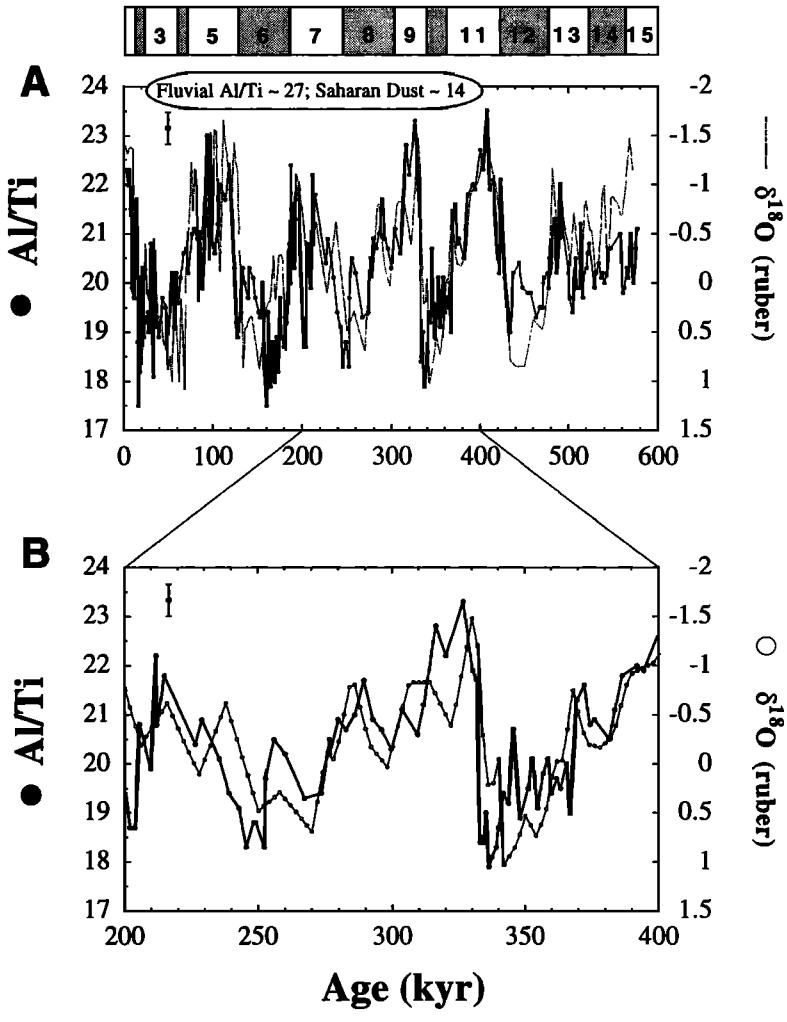

Figure 3. (a) Bulk Al/Ti and $\delta^{18}O$ versus age for the entire record at site 1002. (b) Bulk Al/Ti and $\delta^{18}O$ versus age for the 200-400 kyr portion of Figure 3a. Note the extremely consistent behavior between these two parameters (even taking into account the different sample intervals). Glacial and interglacial (shaded) stages are from *Imbrie et al.* [1984]. See text for discussion of the inferred fluvial Al/Ti ratios of Venezuelan rivers draining into Cariaco. Representative analytical uncertainty of Al/Ti is shown in top left-hand corner of each figure. $\delta^{18}O$ is plotted at 2 kyr steps as interpolated from the higher-resolution age model of *Peterson et al.* [2000].

average ~0.43 (0.41-0.44) [*Longa and Bonilla*, 1987], a value identical to that of average upper crust (0.43) [*Taylor and McLennan*, 1985]. The Al/Ti ratio is also likely to be broadly similar to the average upper crust of Al/Ti ~ 27. The maximum Al/Ti values in the Cariaco Basin are 23-24 (Figure 3). Without additional fluvial data, we cannot resolve whether the Al/Ti ratio of the current fluvial input is truly 27 or is closer to the value of 22 found in the uppermost sediments. Regardless, the sediment in the Cariaco Basin is slightly Ti-rich at all times, with respect to average upper crust. During glacials, as discussed below, the sediments are even more enriched in Ti.

Because of the lack of Ti data, K/Al is more useful for a discussion of the detrital load carried by local rivers. The K/Al ratio of Cariaco Basin sediments decreases during glacial periods (Figure 6). This seems counterintuitive given the increased aridity of glacial periods in general, but it is consistent with the mineralogic observations of *Clayton et al.* [1999], who show that the illite/kaolinite ratio decreases during glacials in the Cariaco Basin. However, because *Longa and Bonilla* [1987] report that sediments from the Laguna de Unare on the coast south of the basin are rich in kaolinite, consistent with kaolinite being a product of chemical weathering in humid, tropical climates [e.g., *Bonatti and Gartner*, 1973], the decrease in K/Al suggests an increase in both the relative abundance of kaolinite and the relative importance, at least for the K budget, of local fluvial sources during glacial periods. We interpret this as reflecting that hemipelagic input from local Venezuelan rivers is more significant in the Cariaco Basin during glacials, since it is the only source region with a direct pathway into the basin during times of increased relative isolation caused by lowered sea level. Thus, during glacials, the locally derived, kaolinite-rich (low K/Al) material is most significant.

This hypothesis is supported by the close cross-spectral relationship between K/Al and the concentration of $CaCO_3$ (Table 2). *Peterson et al.* [1991] argued that the production of

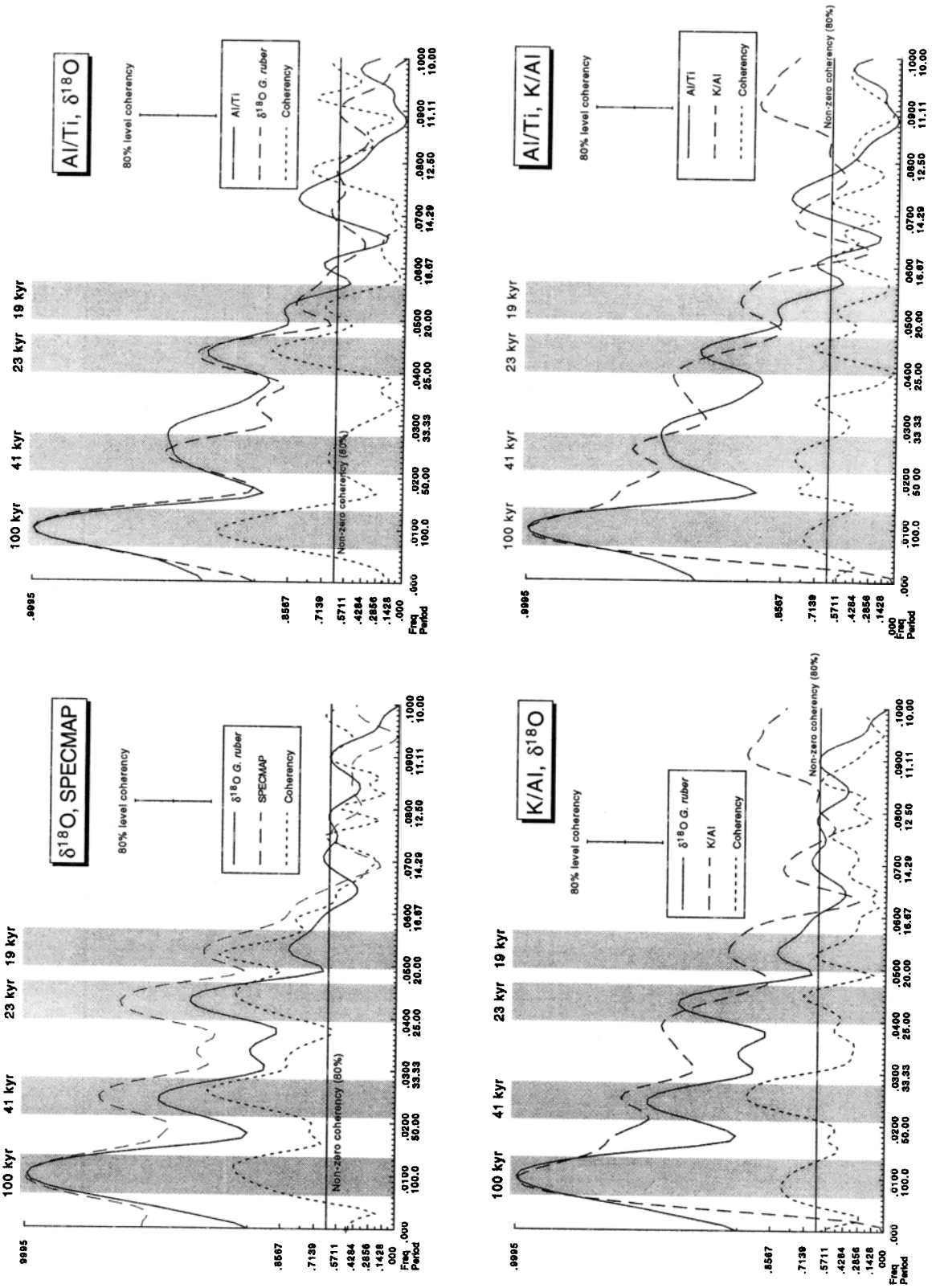

Figure 4. Cross spectral analyses, site 1002. See Table 2.

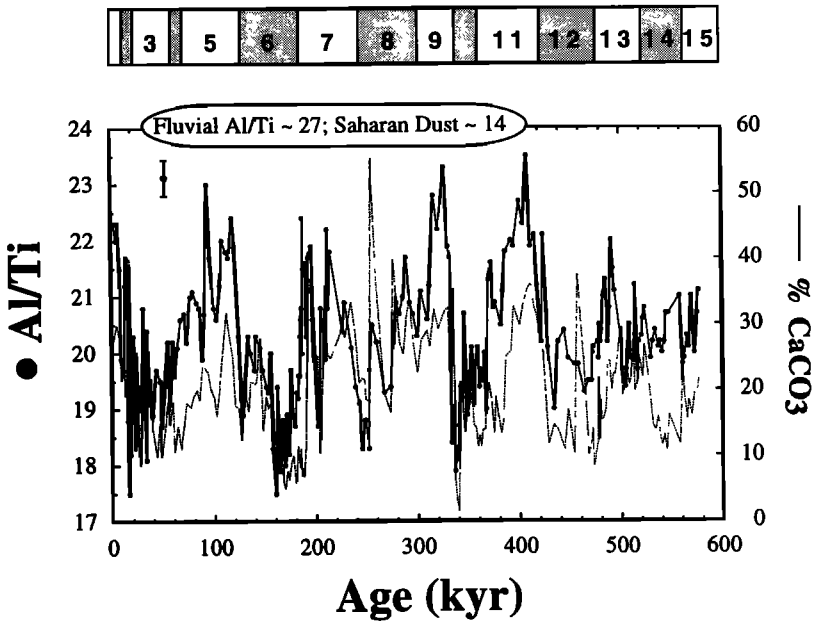

Figure 5. Bulk Al/Ti and $CaCO_3$ versus age at site 1002 Glacial and interglacial (shaded) stages are from *Imbrie et al.* [1984] Representative analytical uncertainty of Al/Ti is shown in the top left-hand corner.

$CaCO_3$ is controlled largely by variations in nutrient supply that are regulated by sea level changes, with biogenic production being minimized during sea level low stands owing to the advection of nutrient-poor waters into the Cariaco Basin. Because K/Al is exactly phase-locked with $\%CaCO_3$ in all spectral frequencies except for the 23 kyr band, it appears most likely that the K/Al variations are also responding to sea level change. Furthermore, because cross-spectral analyses indicates that Al/Ti consistently lags K/Al in the 100 kyr and 41 kyr bands and is unrelated at the higher frequencies (Table 2), it appears that different mechanisms are responsible for the temporal distributions of these two ratios in Cariaco sediment. The difference in the K/Al and Al/Ti temporal signatures, however, need not be related solely to differences in transport

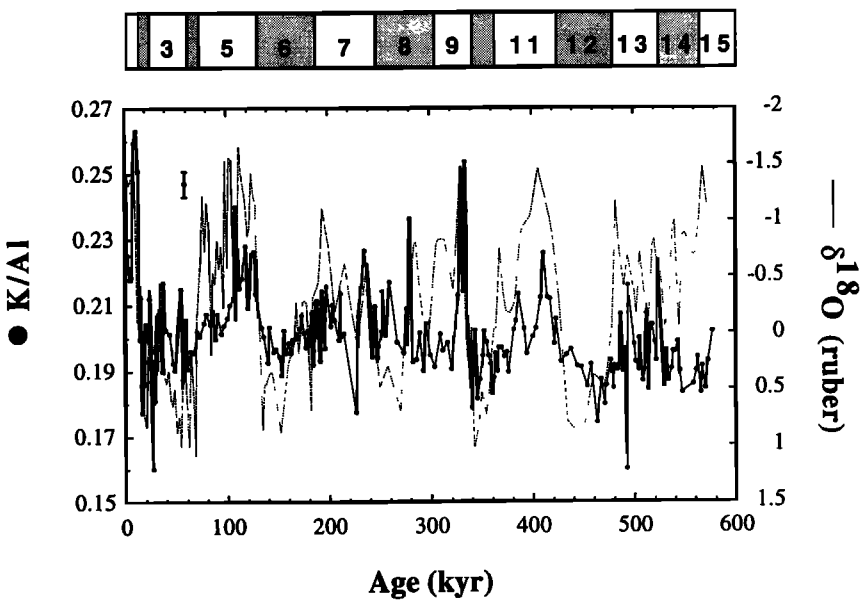

Figure 6. K/Al plotted downcore against $\delta^{18}O$. Glacial and interglacial (shaded) stages are from *Imbrie et al* [1984]. Representative analytical uncertainty of K/Al is shown in the top left-hand corner. $\delta^{18}O$ is plotted at 2 kyr steps as interpolated from the higher-resolution age model of *Peterson et al.* [2000].

mechanism or location of their respective sources, but could also reflect variability in the sum combination of sediment production and transport pathway.

6.3. Potential Marine Transport From the Amazon and Orinoco Rivers

During glacial periods, when the sills surrounding the Cariaco Basin became increasingly more shallow, sediment from the Amazon and Orinoco Rivers that travels along the eastern and northern coast of South America and into the Caribbean Sea [e.g., *Bowles and Fleischer*, 1985] during high sea level stands would be inhibited from intruding into the Cariaco Basin. We here assess the capability of the Amazon and Orinoco Rivers to influence the Al/Ti signature of the Caribbean Sea during either glacials or interglacials.

Al/Ti values for both the Amazon and Orinoco Rivers (Table 1) are low (~16 and ~13, respectively) [*Taylor and McLennan*, 1985; *Martin and Meybeck*, 1979; *Eisma et al.*, 1978]. These Al/Ti values are lower than the reported Al/Ti of average upper crust (~27) [*Taylor and McLennan*, 1985] and the inferred Al/Ti of Laguna de Unare and are lower than even the minimum sedimentary Al/Ti in Cariaco. To increase our confidence in identifying Amazon/Orinoco sources with respect to Al/Ti, we note that Fe/Al values for both the Amazon (~0.48) [*Martin and Meybeck*, 1979; *Taylor and McLennan*, 1985] and Orinoco (~0.51) [*Martin and Meybeck*, 1979] are higher than those of Laguna de Unare (~0.43) [*Longa and Bonilla*, 1987] and average upper crust (~0.43) [*Taylor and McLennan*, 1985], but are similar to that of Post Archean Average Shale (PAAS) (~0.51) [*Taylor and McLennan*, 1985]. Thus, even inferred Al/Ti values for the Amazon and Orinoco Rivers are similar to the reported values above, which are also similar to that of PAAS (~17) [*Taylor and McLennan*, 1985].

The low Al/Ti values for the Amazon and Orinoco rivers should therefore result in low Al/Ti values in Cariaco, were these rivers supplying material to Cariaco during the interglacial periods of high sea levels. Cariaco Al/Ti values, however, are higher during interglacials. Therefore, if Cariaco Al/Ti were tracing Amazon/Orinoco sources, this would require greater Amazon/Orinoco input during glacials, periods of low sea level. This inference is inconsistent both with the K/Al data and with the mineralogic studies of *Clayton et al.* [1999], who found the relative significance of Amazon and Orinoco sediment to increase during interglacials, with Amazon sediment being more prominent than Orinoco sediment [see also *Bowles and Fleischer*, 1985]. Thus, the changes in Cariaco Al/Ti cannot be explained by changes in significance of the Amazon/Orinoco inputs.

6.4. Potential Eolian Transport Pathways

Given the above, we explore the potential for eolian fractionation and transport mechanisms to explain all or some of the observed changes in bulk Al/Ti. During interglacials, when the ITCZ is at its northernmost position, the northeasterly trade winds transport dust to the tropical North Atlantic and Caribbean from African deserts in latitudes above 20°N, namely, the north and central Sahara, in a path between 10° and 25°N, as collectively reported by *Delany et al.* [1967], *Prospero and Nees* [1977], *Prospero et al.* [1981], and *Lisitzin* [1996]. During glacials, when the ITCZ occupies a more southerly average position, the northeasterly trade winds transport African dust from latitudes below 20°N in a transport path between 5° and 15°N [see *Balsam et al.*, 1995]. This region includes the southern Sahara, the sub-Saharan, and Sahel Desert regions. *Balsam et al.* [1995] observed a greater abundance of iron-stained quartz from the southern Sahara and Sahel Desert regions in the glacial dust plume, while the interglacial dust plume contained greater clear quartz from the northern and central Sahara. Thus, during glacials, dust input from Africa reaches a maximum over the western equatorial Atlantic [e.g., *Sarnthein*, 1978; *Prospero et al.*, 1981; *Sarnthein et al.*, 1981; *Pokras and Mix*, 1987; *Balsam et al.*, 1985].

Saharan dust is rich in Ti [*Schutz and Rahn*, 1982], with minimum values of Al/Ti ~ 11 (Table 1) (e.g., from the northeastern Sahara [*Ganor et al.*, 1991]). *Glaccum* [1978] and *Glaccum and Prospero* [1980] studied the mineralogy and chemistry of Saharan-sourced aerosols gathered in the Cape Verdes Islands (Al/Ti ~ 14), Barbados (Al/Ti ~ 13), and Miami (Al/Ti ~14). Recall that on the basis of comparisons of the local fluvial Fe/Al ratio to that of average crust, as well as a review of the local geology, there appear to be no local sources of detrital material with the appropriate Al/Ti ratio to explain Cariaco Al/Ti. Cognizant of the caveat that the local fluvial Al/Ti ratio has not been directly measured, we nonetheless feel the sedimentary Al/Ti data are best explained as recording the influence of Saharan-sourced, Ti-rich eolian material, particularly for the strong climatically linked Al/Ti variability in the 100 kyr band. The cross-spectral data (Table 2) indicate that in this band the maximum input of Ti occurs exactly at the glacial maximum. Our data suggest that increased wind strength or aridity (e.g., increasing extent of dune sands) [*Sarnthein*, 1978], or both, during glacial periods in the 100 kyr band leads to an increase in the input of Ti-rich Saharan material. This results in a lowering of the bulk sedimentary Al/Ti ratio.

Our interpretation of a Saharan-derived eolian source being responsible for at least part of the Ti-rich composition of Cariaco sediment is supported by the chemical and mineralogic data of *Glaccum* [1978] and *Glaccum and Prospero* [1980]. In addition to documenting the low Al/Ti in Saharan-sourced aerosols in the Cape Verde Islands, Barbados, and Miami, *Glaccum* [1978, p. 92] observed that Ti was contained in "micron-sized needles of rutile." Thus the chemistry and the mineralogy of the aerosol confirm the presence of an extremely Ti-rich phase (that is, rutile), variability of which can easily cause large changes in the bulk Al/Ti ratio, as will be quantified below. *Glaccum* [1978] and *Glaccum and Prospero* [1980] suggest that the Ti enrichment in the tropical North Atlantic aerosols is caused by progressive size sorting, with the clay-associated rutile in the fine fraction of the aerosol increasing with lateral distance from the source.

These observations have ramifications for understanding the nature of eolian transport of heavy minerals to the ocean. In the following discussion, it is important to differentiate

between relative and absolute grain size comparisons. While it is clear that Ti is contained in heavy mineral phases, monsoonal climate signals in the Indian Ocean [*Shimmield et al.*, 1990; *Shimmield and Mowbray*, 1991; *Weedon and Shimmield*, 1991] suggest that decreases in Al/Ti can be explained by grain size fractionations with Ti-rich matter being relatively coarse in size, although grain size distributions were not quantified in these chemical sample sets and the Ti-to-coarse-fraction link was based on results from the literature on aqueous transport and deposition. *Boyle* [1983] observed that 85-90% of the sediment in his study in the eastern equatorial Pacific Ocean was contained in the < 6 μm size, with 45-70% being even < 2 μm, and noted that the control of Al/Ti must be in these finer grain sizes. *Rea* [1994] also observed that ~95% of typical eolian material in pelagic sediments is <6-8 μm. Therefore, any coarsening of the Ti inventory must exist as a gradation essentially entirely within these finest size fractions. The previously published data sets combined with the Cariaco results indicate that the control of Al/Ti in sediment is most likely in the finest grain size fractions, and yet may reflect a very subtle grain size gradation within these finest fractions. The hypothesis that the rutile is contained in the finest fraction can be tested by future studies of grain size variations within Cariaco sediment that attempt to target grain size distributions within these finest fractions (if analytically possible, see discussion by *Rea* [1994]). Regardless of how the precise chemical-grain size associations are resolved, however, it will not affect the underlying fact that the eolian material transported across the tropical Atlantic to the Caribbean is enriched in rutile and thus Ti.

Accordingly, our data can be explained by invoking that, during glacial periods, more Ti-rich African dust is available owing to increased wind strength or aridity, or both, which creates more Ti-rich eolian material due to grain size fractionation reflecting wind strength changes or flux changes associated with variations in aridity and source area [e.g., *Sarnthein*, 1978; *Rea*, 1994]. During interglacial periods, either less eolian material or less fractionated eolian material will be transported across the Atlantic, and the Al/Ti ratio would not be as affected by the Ti-rich Saharan inputs. Thus, Al/Ti ratios would be more similar to those of the more local fluvial sources, which as stated above, are likely to be similar to average upper crust (Al/Ti ~ 27) or to the near-surface sediments (Al/Ti ~ 22). Notwithstanding the uncertainty of the chemical-grain size associations of the Ti-bearing phase, as discussed above, the effect of enhanced winds on Al/Ti has also been observed at sites in the equatorial Pacific and the Arabian Sea, where *Boyle* [1983], *Shimmield et al.* [1990], *Shimmield and Mowbray* [1991], and *Weedon and Shimmield* [1991] showed decreased Al/Ti during glacial periods.

6.5. Titanium Mass Balance: Accumulation Rates of Rutile

Is our interpretation of eolian input causing the sedimentary variability consistent with a mass balance based on eolian fluxes from the Sahara to the tropical North Atlantic? Using end-member values of local fluvial input (inferred Al/Ti ~ 27) and the chemical eolian data of *Glaccum* [1978] (with Al/Ti ~ 13 at Barbados), one could potentially conclude that upward of 35% (for interglacials, to lower the sedimentary Al/Ti to ~ 22; Figure 3) or 65% (for glacials, to lower the sedimentary Al/Ti to ~ 18; Figure 3) of the bulk sediment is composed of eolian material. These are most likely unrealistically large eolian contributions to this nearshore basin, but it is important to note that this calculation assumed an eolian end-member of the current aerosol ratio. However, examination of accumulation rates, and the effect of variation of the amount of rutile in an end-member, yields important information. Considering the average concentrations of Al and Ti in the youngest four samples (selected because they are likely to be the most appropriate to compare to modern data sets), we can calculate an "excess Ti" concentration that quantifies the enrichment of Ti in these samples with respect to the inferred fluvial Al/Ti ~ 27. This is calculated according to

$$Ti_{excess} = Ti_{total} - [Al_{sample} \times (Ti/Al)_{fluvial}]$$

and yields a value of ~ 450 ppm Ti_{excess}. Using an average Cariaco sedimentation rate of 30 cm ky^{-1} [*Peterson et al.*, 2000] and a representative dry bulk density of 0.85 g cm^{-3}, we calculate the accumulation rate of the Ti_{excess} to be 0.0060 g cm^{-2} kyr^{-1}. This value is only 0.046% of the total terrigenous accumulation rate of ~ 15 g cm^{-2} kyr^{-1} at Cariaco (determined using the same sedimentation rate and dry bulk density, along with a representative concentration of terrigenous matter from Figure 2). The identical calculation for the most recent glacial period (using data from 17.243 kyr to 19.840 kyr in Table 3) yields the value of 0.119% of the total terrigenous accumulation potentially being caused by rutile. Both calculations indicate a realistically small amount of rutile can greatly affect the sedimentary Al/Ti ratio. These calculations, however, consider the total sedimentation accumulation, not the accumulation of the eolian component. Using a similar strategy in terms of accumulation rates and representative densities, *Glaccum* [1978] calculated that the input of Saharan-derived eolian material would result in an average tropical North Atlantic pelagic sedimentation rate of 11 mm kyr^{-1}. Although this is an average for the tropical North Atlantic (and thus the Caribbean rate is likely to be lower), this 11 mm kyr^{-1} translates to 0.935 g cm^{-2} kyr^{-1}, or 6% of the total terrigenous accumulation rate. The inferred interglacial and glacial accumulation rates of Ti_{excess} calculated above in turn can be considered as 0.6% and 2%, respectively, of this 0.935 g cm^{-2} kyr^{-1}. *Glaccum* [1978] notes that "accessory minerals" (minerals other than quartz, plagioclase, illite, kaolinite, calcite, and dolomite) can account for 1-3% of the total aerosol inventory and commonly emphasizes the presence of rutile in the aerosols (although he did not quantify its abundance). While we do not suggest that all of the 1-3% accessory phases is composed of rutile, it appears that within the tolerances of the calculations, regardless of the approach, very small amounts of eolian rutile, such as even a fraction of this 1-3% "accessory" inventory or very subtle changes in the amount of rutile from glacial to interglacial, can potentially explain variations in the bulk Al/Ti ratio of sediment deposited in a hemipelagic regime.

6.6. Combined Eolian and Fluvial Control of Al/Ti?

Any climatological proxy, be it chemical or sedimentological in nature, need not be responding to the same forcing functions at all Milankovitch frequencies. For example, *Rea* [1994] notes that global aridity variations, as recorded by eolian mass accumulation rates, tend to show strongest cyclicity in the 100 kyr band along with lesser spectral power in the higher Milankovitch frequencies of 41 kyr, 23 kyr, and 19 kyr. Eolian grain size records of wind intensity also display 100 kyr power, but such power is usually of secondary importance to that at higher Milankovitch frequencies. Wind intensity and aridity signals are commonly decoupled [*Rea*, 1994].

If the Cariaco Al/Ti variation is, in fact, due to eolian processes, on the basis of the chemical measurements alone we are unable to identify whether changes in eolian flux or mean grain size, commonly ascribed to changes in source area aridity and wind strength, respectively [e.g., *Rea*, 1994], are the dominant controlling mechanism of the sedimentary Al/Ti ratio. We are particularly limited to this end because we do not have accumulation rate data available for Cariaco sedimentation at this ODP site. Comparing the temporal patterns of Al/Ti variability to the general eolian summaries of *Rea* [1994] suggests that the Cariaco Al/Ti is a mixed aridity/intensity signal. The study of *Tiedemann et al.* [1994], at ODP site 659 located immediately downwind of the Sahara, also provides useful constraints. *Tiedemann et al.* [1994] assumed that the noncarbonate material at their site was composed of eolian material, which is reasonable given the lithostratigraphy but also implies that their records could be affected by carbonate dissolution. Nonetheless, these workers suggested that the Saharan dust flux over the past 500 kyr shows strong spectral density at 100 kyr and 41 kyr, with considerably less strength in the 23 kyr band. They also documented that the strongest cross-spectral relationships between dust flux and $\delta^{18}O$ occur in the 41 kyr and 23 kyr bands and suggested that dust flux behavior in the 41 kyr band was best explained by variations in aridity. Both *Tiedemann et al.* [1994] and our data show spectral density at 100 kyr, although in Cariaco the spectral behavior of Al/Ti is extremely closely linked to $\delta^{18}O$ (Table 2), whereas in the eastern Atlantic it is not related. Both our study and that of *Tiedemann et al.* [1994] show strong spectral density at the 41 kyr and 23 kyr bands, with both being coherent with $\delta^{18}O$. Thus, Al/Ti in the Cariaco Basin may be responding to a combination of wind strength and source aridity.

Our earlier discussions ruling out local fluvial sources of Ti-rich material are based on chemical comparisons, and we feel they are strong arguments against a local source of Ti-rich material. Nonetheless, these arguments are limited in that, although all available means have been used to accurately approximate the Al/Ti value of local sources, no direct measurements have been made. There is nonchemical evidence (i.e., spectral relationships) in favor of a local control of sedimentary Al/Ti in the non-100 kyr Milankovitch bands. In the 100 kyr band, the exactly in-phase cross-spectral relationship between Al/Ti and planktonic $\delta^{18}O$ in the Cariaco Basin (Table 2) is consistent with higher wind speeds and/or aridity in the 100 kyr band transporting Ti-rich eolian material to the Cariaco Basin from the Sahara. Because the Al/Ti and K/Al records have a lead/lag relationship (Table 2), this eolian assignment for the 100 kyr mechanism is also consistent with K/Al (and the illite/kaolinite data of *Clayton et al.* [1999]) being spectrally linked with no phase angle to $\%CaCO_3$, which has been previously suggested to respond to sea level changes [*Peterson et al.* 1991].

However, in the 41 kyr, 23 kyr, and 19 kyr bands, Al/Ti significantly leads $\delta^{18}O$, and it is difficult in terms of cause and effect to develop an eolian mechanism that preceeds the peak climatic condition by such a long time (Table 2). The Al/Ti-$\delta^{18}O$ cross-spectral relationship in Cariaco indicates that the maximum relative Ti input is occurring at the maximum rate of sea level fall, which is also during the maximum rate of exposure of the continental shelf regions, yet prior to the shelves being highly vegetated. Such a period is likely to be when the Cariaco Basin would receive the greatest influx of hemipelagic sediment. Thus, if our inferred local Al/Ti values are shown to be inappropriate and a very local Ti-rich source is eventually found in the immediate Venezuelan region, a transport pathway exists to move this material into the Cariaco Basin. Laterization, which occurs during tropical soil production, preferentially concentrates refractory elements (including both Al and Ti), and thus in a closed system weathering will not significantly affect their ratio. Interestingly, if an appropriate eolian source is active, lateritic soils can become enriched in rutile and thus Ti [*Brimhall et al.*, 1988], and so a speculative Ti-rich soil in the Cariaco region may in fact reflect eolian input from the Sahara regardless. Nonetheless, until a local source is found to match the chemical signatures, we remain constrained by the inferred values and the lack of appropriate geological formations to supply Ti-rich material, and therefore the direct eolian input of rutile appears to be the most plausible mechanism to decrease the bulk sedimentary Al/Ti to the observed values at site 1002.

7. Summary

The results from elemental geochemical analyses of the bulk sediment from Cariaco Basin site 1002 indicate climatically sensitive variations in the Al/Ti and K/Al ratios of the terrigenous sediment fraction. During glacial periods, owing to increased basin isolation, the marine input of terrigenous sediment to the Cariaco Basin records input from local Venezuelan rivers, as indicated by a decrease in K/Al (Figure 7). This assumes that K/Al is representative of illite/kaolinite, which is consistent with local tropical fluvial sources being rich in kaolinite [*Longa and Bonilla*, 1987]. Our chemical interpretations are also consistent with and corroborate the clay mineralogic observations of *Clayton et al.* [1999].

The decrease in Al/Ti during glacial periods is more difficult to explain. There are no published Ti data for the local rivers draining into the Cariaco Basin, and thus, although all available means have been used in this paper to accurately approximate the Al/Ti value of these local sources, no direct

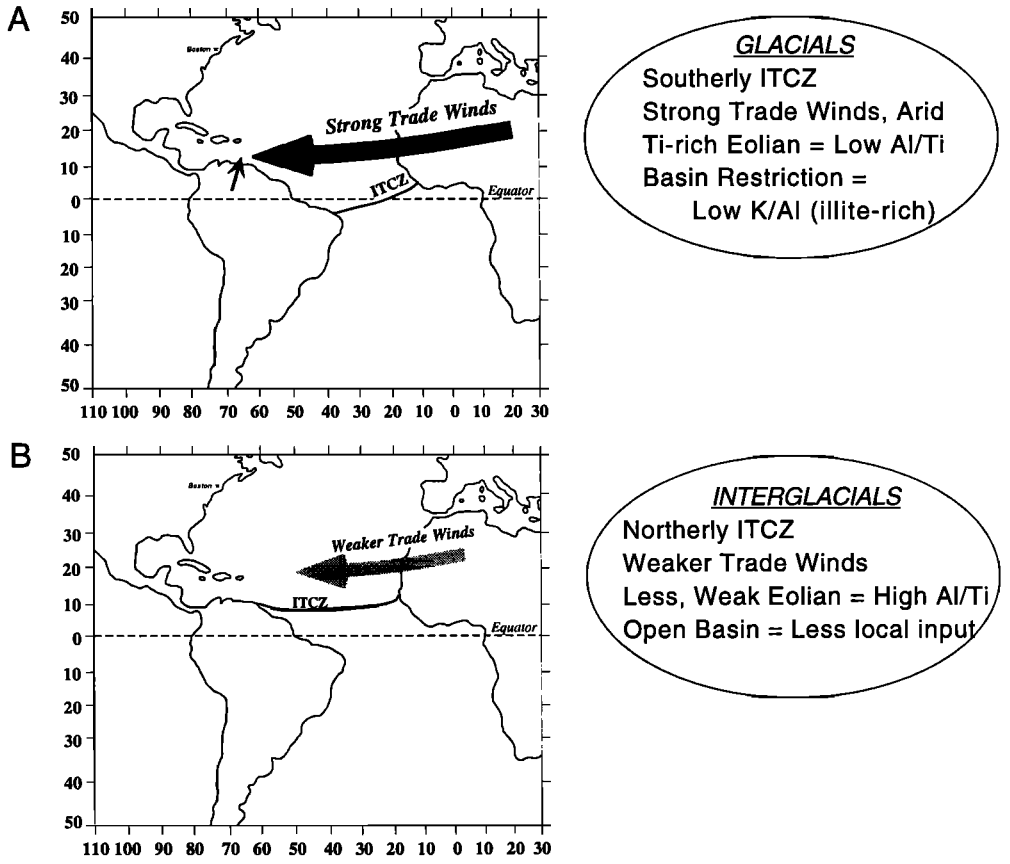

Figure 7. Summary of depositional processes controlling the variations of Al/Ti and K/Al at site 1002 in the Cariaco Basin during (a) glacial and (b) interglacial periods.

measurements have been made. Working with average crustal values, which are consistent with the few non-Ti data in the local fluvial sources, and on the basis of a survey of the local geology, it appears that local inputs are not of the appropriate chemical composition to explain the sedimentary Al/Ti at site 1002. Thus we instead suggest that the sedimentary Al/Ti is indicative of variations in eolian processes that enrich the relative fraction of Saharan-derived Ti-bearing phases (Figure 7). Al/Ti may be a useful tracer of eolian provenance since dune sands of the northern Sahara, which increase in extent during glacial periods caused by increased aridity [e.g, *Prospero and Nees*, 1977; *Sarnthein*, 1978], are enriched in Ti and heavy minerals [*Schutz and Rahn*, 1982, and references therein; *Ganor et al.*, 1991]. While we cannot resolve with chemical data alone whether the relative increase in Ti reflects a flux change (recording changes in source aridity, [*Rea*, 1994]) or a grain size change (recording a change in wind strength, [*Rea*, 1994]), our chemical interpretations are consistent with various other studies documenting general glacial increases in aridity and eolian transport [e.g,. *Prospero and Nees*, 1977; *Tiedemann et al.*, 1994, *Balsam et al.*, 1995, and references therein], as well as those of the mineralogy and chemistry of Saharan-derived dust transported across the tropical North Atlantic [e.g., *Glaccum*, 1978; *Glaccum and Prospero*, 1980]. We are able to close a mass balance based on eolian and terrigenous mass accumulation rates by documenting that very small, and geologically reasonable, changes in rutile accumulation can explain the observed increases and decreases in bulk sedimentary Al/Ti.

To conclude, we have shown that relatively simple chemical analyses of the bulk sediment in tropical marine sedimentary sequences can yield important information regarding late Pleistocene climate change. Future work should aim to characterize the eolian material, specifically, the Al and Ti concentrations, from the northern, central, and southern Sahara and Sahel Deserts, in order to help constrain the mechanisms responsible for the glacially low Al/Ti, and also further target sedimentological-chemical associations within the Cariaco Basin. Future integrations of chemical and mineralogical data in these sediments are likely to be highly fruitful. This study, which documents changes in eolian input and fluvial provenance in the Cariaco Basin at the relatively low Milankovitch frequencies, should provide a quantitative baseline from which chemical studies at higher, sub-Milankovitch timescales can provide insight into higher-frequency climate change.

Acknowledgments. We thank T. Clayton and R. Pearce for very kindly sharing their clay mineral data and publication preprint. S. Hovan and P. Delaney provided detailed comments on this manuscript during review, and their comments greatly focused our arguments. D. Murray

of Brown University provided insightful suggestions on an early version of the manuscript, and postreview conversations with S. Hovan, S. Clemens, E. Arnold, and M. Leinen greatly helped us begin down the long road toward understanding the intricacies of interpreting eolian records. R.W.M. and L.C.P. acknowledge financial support from USSSP postcruise funding and from NSF grant OCE-9709807 (to L.C.P.). Acquisition and initial maintenance of the JY170C ICP-ES facility at Boston University were supported by NSF EAR-9724282. K.M.Y. thanks Boston University for graduate student support. We collectively express our gratitude to A. Jamil, M. Evonuk, and J. Sparks for their assistance in the Analytical Geochemistry Laboratory at Boston University and S. Rutherford at URI and P. Howell at Brown University for consultation regarding the spectral analyses. Table 3 is also available electronically from the corresponding author (R.W.M.).

References

Balsam, W.L., B.L. Otto-Bliesner, and B.C. Deaton, Modern and Last Glacial Maximum eolian sedimentation patterns in the Atlantic Ocean interpreted from sediment iron oxide content, *Paleoceanography, 10*, 493-507, 1995.

Banakar, V.K., G. Parthiban, J.N. Pattan, and P. Jauhari, Chemistry of surface sediment along a north-south transect across the equator in the Central Indian Basin: An assessment of biogenic and detrital influences on elemental burial on the seafloor, *Chem. Geol., 147*, 217-232, 1998.

Banks, P.O., Basement rocks bordering the Gulf of Mexico and the Caribbean Sea, in *The Ocean Basins and Margins: Vol. 3, The Gulf of Mexico and the Caribbean*, edited by A.E.M. Nairn and F.G. Stehli, pp. 181-199, Plenum, New York, 1975.

Biju-Duval, B., A. Mascle, H. Rosales, and G. Young, Episutural Oligo-Miocene basins along the north Venezuelan margin, in *Studies in Continental Margin Geology*, edited by J.S. Watkins and C.L. Drake, *AAPG Mem. 34*, pp. 347-358, 1982.

Bonatti, E., and S. Gartner, Jr., Caribbean climate during Pleistocene Ice Ages, *Nature, 244*, 563-565, 1973.

Bowles, F.A., and P. Fleischer, Orinoco and Amazon River sediment input into the eastern Caribbean Basin, *Mar. Geol., 68*, 53-72, 1985.

Boyle, E.A., Chemical accumulation variations under the Peru Current during the past 130,000 years, *J. Geophys. Res., 88*, 7667-7680, 1983.

Brimhall, G.H., C.J. Lewis, J.J. Ague, W.E. Dietrich, J. Hampel, T. Teague, and P. Rix, Metal enrichment in bauxites by deposition of chemically mature aeolian dust, *Nature, 333*, 819-824, 1988.

Clayton, T., R.B. Pearce, and L.C. Peterson, Indirect climatic control of the clay mineral composition of Quaternary sediments from the Cariaco Basin, northern Venezuela (ODP site 1002), *Mar. Geol., 161*, 191-207, 1999.

Condie, K.C., Chemical composition and evolution of the upper continental crust: Contrasting results from surface samples and shales, *Chem. Geol., 104*, 1-37, 1993.

Damuth, J.E., and R.W. Fairbridge, Equatorial Atlantic deep-sea arkosic sands and ice-age aridity in tropical South America, *Geol. Soc. Am. Bull., 81*, 189-206, 1970.

Delaney, A.C., D.W. Parkin, J.J. Griffin, E.D. Goldberg, and B.E.F. Reimann, Airborne dust collected at Barbados, *Geochim. Cosmo. Acta, 31*, 885-909, 1967.

deMenocal, P.B., W.F. Ruddiman, and E.M. Pokras, Influences of high- and low-latitude processes on African terrestrial climate: Pleistocene eolian records from equatorial Atlantic Ocean Drilling Program site 663, *Paleoceanography, 8*, 209-242, 1993.

Donnelly, T.W., et al., History and tectonic setting of Caribbean magmatism, in *The Caribbean Region, Geol. North Am.*, vol. H, edited by G. Dengo and J.E. Case, pp. 339-374, Geol. Soc. Am., Boulder, Colo., 1990.

Duce, R.A., et al., The atmospheric input of trace species to the world ocean, *Global Biogeochem. Cycles, 5*, 193-259, 1991.

Dymond, J., R. Collier, J. McManus, S. Honjo, and S. Manganini, Can the aluminum and titanium contents of ocean sediments be used to determine the paleoproductivity of the oceans?, *Paleoceanography, 12*, 586-593, 1997.

Eisma, D., S.J. van der Gast, J.M. Martin, and A.J. Thomas, Suspended matter and bottom deposits of the Orinoco delta. Turbidity, mineralogy, and elementary composition, *Neth. J. Sea Res., 12*, 224-251, 1978.

Ganor, E., H.A. Foner, S. Brenner, E. Neeman, and N. Lavi, The chemical composition of aerosols settling in Israel following dust storms, *Atmos. Environ., Part A, 25*, 2665-2670, 1991.

Glaccum, R.A., The mineralogical and elemental composition of mineral aerosols over the tropical North Atlantic: The influence of Saharan dust, M.S. thesis, 161 pp. pp., Univ. of Miami, Miami, Florida, 1978.

Glaccum, R.A., and J.M. Prospero, Saharan aerosols over the tropical North Atlantic--Mineralogy, *Mar. Geol., 37*, 295-321, 1980.

Hastenrath, S., and P.J. Lamb, *Climatic Atlas of the Tropical Atlantic and Eastern Pacific Oceans*, Univ. Wis. Press, Madison, 1977.

Haug, G., T.F. Pedersen, D.M. Sigman, S.E. Calvert, B. Nielsen, and L.C. Peterson, Glacial/interglacial variations in production and nitrogen fixation in the Cariaco Basin during the last 580 kyr, *Paleoceanography, 13*, 427-432, 1998.

Hovan, S.A., and D.K. Rea, The Cenozoic record of continental mineral deposition on Broken and Ninetyeast Ridges, Indian Ocean: Southern African aridity and sediment delivery from the Himalayas, *Paleoceanography, 7*, 833-860, 1992.

Hovan, S.A., D.K. Rea, and N.G. Pisias, Late Pleistocene continental climate and oceanic variability recorded in northwest Pacific sediments, *Paleoceanography, 6*, 349-370, 1991.

Hughen, K.A., J.T. Overpeck, L.C. Peterson, and R.F. Anderson, The nature of varved sedimentation in the Cariaco Basin, Venezuela, and its paleoclimatic significance, in *Palaeoclimatology and Palaeoclimatology from Laminated Sediments*, edited by A.E.S. Kemp, *Geol. Soc. Spec. Publ., 116*, , 1996.

Imbrie, J., J.D. Hays, D.G. Martinson, A. McIntyre, A.C. Mix, J.J. Morley, N.G. Pisias, W.L. Prell, and N.J. Shackleton, The orbital theory of Pleistocene climate: Support from a revised chronology of the marine $\delta^{18}O$ record, in *Milankovitch and Climate, Part 1*, edited by A.L. Berger and e. a., pp. 269-305, Reidel, 1984.

Johnsson, M.J., R.F. Stallard, and N. Lundburg, Controls on the composition of fluvial sands from a tropical weathering environment: Sands of the Orinoco River drainage basin, Venezuela and Columbia, *Geol. Soc. Am. Bull., 103*, 1622-1647, 1991.

Leinen, M., The late Quaternary record of atmospheric transport to the Northwest Pacific from Asia, in *Paleoclimatology and Paleometeorology: Modern and Past Patterns of Global Atmospheric Transport*, edited by M. Leinen and M. Sarnthein, pp. 693-732, Kluwer Acad., Norwell, Mass., 1989.

Leinen, M., D. Cwienk, G.R. Heath, P.E. Biscaye, V. Kolla, J. Thiede, and J.P. Dauphin, Distribution of biogenic silica and quartz in recent deep-sea sediments, *Geology, 14*, 199-203, 1986.

Liotard, J.M., H.G. Barsczus, D. Dupuy, and J. Dostal, Geochemistry and origin of basaltic lavas from Marquesas Archipelago, French Polynesia, *Contrib. Mineral. Petrol., 92*, 260-268, 1986.

Lisitzen, A.P., *Oceanic Sedimentation: Lithology and Geochemistry*, edited by J.P. Kennett, 400 pp., AGU, Washington, D.C., 1996.

Longa, Y., and J. Bonilla, Caracterizacion quimica de los sedimentos de la interfase de la Laguna de Unare, Venezuela, *Bol. Inst. Oceanogr. Univ. Oriente, 26*, 81-89, 1987.

Martin, J.M., and M. Meybeck, Elemental mass-balance of material carried by the major world rivers, *Mar. Chem., 7*, 173-206, 1979.

Murray, R.W., and M. Leinen, Scavenged excess Al and its relationship to bulk Ti in biogenic sediment from the Central Equatorial Pacific Ocean, *Geochim. Cosmochim. Acta, 60*, 3869-3878, 1996.

Murray, R.W., M. Leinen, and A.R. Isern, Biogenic flux of Al to sediment in the Central Equatorial Pacific Ocean: Evidence for increased productivity during glacial episodes, *Paleoceanography, 8*, 651-670, 1993.

O'Brien, S.R., P.A. Mayewski, L.D. Meeker, D.A. Meese, M.S. Twickler, and S.I. Whitlow, Complexity of Holocene climate as reconstructed from a Greenland ice core, *Science, 270*, 1962-1964, 1995.

Oppo, D.W., J.F. McManus, and J.L. Cullen, Abrupt climate events 500,000 to 340,000 years ago: Evidence from subpolar North Atlantic sediments, *Science, 279*, 1335-1338, 1998.

Peterson, L.C., J.T. Overpeck, N.G. Kipp, and J. Imbrie, A high-resolution late Quaternary upwelling record from the anoxic Cariaco Basin, Venezuela, *Paleoceanography, 6*, 99-119, 1991.

Peterson, L.C., G.H. Haug, R.W. Murray, K.M. Yarincik, J.W. King, T.J. Bralower, K. Kameo, and R.B. Pearce, Late Quaternary stratigraphy and sedimentation at ODP Site 1002, Cariaco Basin (Venezuela), *Proc. Ocean Drill. Progr. Sci. Res., 165*, in press, 2000.

Pokras, E.M., and A.C. Mix, Earth precession cycle and Quaternary climatic change in tropical Africa, *Nature, 326*, 486-487, 1987.

Prospero, J.M., and R.T. Nees, Dust concentration in the atmosphere of the equatorial North Atlantic: Possible relationship to Sahelian drought, *Science, 196*, 1196-1198, 1977.

Prospero, J.M., R.A. Glaccum, and R.T. Nees, Atmospheric transport of soil dust from Africa to South America, *Nature, 289*, 570-572, 1981.

Raymo, M.E., K. Ganley, S. Carter, D.W. Oppo, and J. McManus, Millenial-scale climate instability during the early Pleistocene epoch, *Nature, 392*, 699-702, 1998.

Rea, D K , The paleoclimatic record provided by eolian deposition in the deep sea· The geologic history of wind, *Rev. Geophys., 32*, 159-195, 1994.

Rea, D.K., and S.A Hovan, Grain size distribution and depositional processes of the mineral component of abyssal sediments: Lessons from the North Pacific, *Paleoceanography, 10*, 251-258, 1995

Rea, D.K., S.A Hovan, and T.R. Janecek, Late Quaternary flux of eolian dust to the pelagic ocean, in *Material Fluxes on the Surface of the Earth*, pp. 116-124, Nat. Res. Counc , Washington, D C., 1994

Rea, D.K., H. Snoeckx, and L.H. Joseph, Late Cenozoic eolian deposition in the North Pacific. Asian drying, Tibetan uplift, and cooling of the northern hemisphere, *Paleoceanography, 13*, 215-224, 1998.

Ruddiman, W.F., and T.R. Janecek, Pliocene-Pleistocene biogenic and terrigenous fluxes at equatorial Atlantic sites 662, 663, and 664, in *Proc. Ocean Drill. Progr. Sci. Res., 108*, ,211-240, 1989

Sarnthein, M , Sand deserts during glacial maximum and climatic optimum, *Nature, 272*, 43-45, 1978.

Sarnthein, M , G Tetzlaff, G. Koopmann, K. Wolter, and U Pflaumann, Glacial and interglacial wind regimes over the eastern sub-tropical Atlantic and northwest Africa, *Nature, 293*, 193-196, 1981.

Schubert, C , The origin of the Cariaco Basin, southern Caribbean Sea, *Mar. Geol , 47*, 345-360, 1982.

Schutz, L., and K A. Rahn, Trace-element concentrations in erodible soils, *Atmos. Environ., 16*, 171-176, 1982

Shimmield, G.B., and S R. Mowbray, The inorganic geochemical record of the northwest Arabian Sea. A history of productivity variation over the last 400 k y from Sites 722 and 724, *Proc Ocean Drill. Program Sci. Res., 117*, 409-429, 1991.

Shimmield, G.B., S.R. Mowbray, and G.P. Weedon, A 350 ka history of the Indian Southwest Monsoon--Evidence from deep-sea cores, northwest Arabian Sea, *Trans. R. Soc. Edinburgh Earth Sci., 81*, 289-299, 1990.

Sigurdsson, H., and e. al., *Proceedings of the Ocean Drilling Program, Initial Reports, Ocean Drilling Program*, vol. 165, Ocean Drill Program, College Station, Tex., 1997

Taylor, S.R , and S M McLennan, *The Continental Crust· Its Composition and Evolution*, 312 pp , Blackwell Sci., 1985.

Thompson, L G., E. Mosley-Thompson, M.E. Davis, P.-N. Lin, K.A. Henderson, J. Cole-Dai, J.F. Bolzan, and K.-B. Liu, Late glacial stage and Holocene tropical ice core records from Huascaran, Peru, *Science, 269*, 46-50, 1995.

Tiedemann, R., M Sarnthein, and N.J. Shackleton, Astronomic timescale for the Pliocene Atlantic $\delta^{18}O$ and dust flux records of Ocean Drilling Program site 659, *Paleoceanography, 9*, 619-638, 1994

Weedon, G P , and G.B. Shimmield, Late Pleistocene upwelling and productivity variations in the northwest Indian Ocean deduced from spectral analyses of geochemical data from Sites 722 and 724, *Proc. Ocean Drill Program Sci. Res., 117*, 431-443, 1991.

R. W. Murray and K. M. Yarincik, Department of Earth Sciences, Boston University, Boston, MA 02215. (rickm@bu.edu; yarincik@bu.edu)

L. C Peterson, Rosenstiel School of Marine and Atmospheric Science, University of Miami, Miami, FL 33149. (lpeterson@rsmas.miami.edu)

(Received January 28, 1999;
evised September 3, 1999;
accepted September 15, 1999.)